# A HAND-HELD MICROFLUIDIC FLUORESCENCE LAB-ON-CHIP BIOLOGICAL DETECTION SYSTEM

**BY**

**JOHN D. JONES**

**A DISSERTATION SUBMITTED IN PARTIAL FULFILLMENT OF THE REQUIREMENTS FOR THE DEGREE OF**

**DOCTOR OF PHILOSOPHY**

**IN**

**MECHANICAL, INDUSTRIAL AND SYSTEMS ENGINEERING**

**UNIVERSITY OF RHODE ISLAND**

**2012**

DOCTOR OF PHILOSOPY DISSERTATION

OF

JOHN D. JONES

APPROVED:

Thesis Committee:

Major Professor Dr. Mohammad Faghri

Dr. Constantine Anagnostopoulos

Dr. Zongquin Zhang

Dr. Geoffrey Bothun

Dr. Nasser H. Zawia
DEAN OF THE GRADUATE SCHOOL

UNIVERSITY OF RHODE ISLAND
2012

## ABSTRACT

This experimental study investigates the feasibility of using a lens-less charge-coupled device (CCD) for the detection of organic and inorganic fluorophores. The study further investigates the feasibility of this device as a detection sensor in a hand-held Point-of-Care (POC) microfluidic Lab-on-Chip (LOC) detector.

The use of microfluidic LOC technology now allows the miniaturization of standard laboratory equipment and helped reduce the time necessary to achieve an accurate result. However, current Point-of-Care (POC) devices are still relatively large and are not easily transportable. For these reasons, the design of a space saving imager has become the target of this study.

In the study, several CCD cameras similar to a webcam with the lens removed were tested for the detection of organic and inorganic fluorophores. Of these, a Fire I CCD lens-less imager, having the ability to return a true representation of the detection site, was successfully used for the detection of three common fluorophores (fluorescein, phosphor dots, and quantum dots). Thus it was shown that the lens-less CCD imager is accurate enough to detect quantum dots in alcohol with a Limit of Detection (LOD) at 0.028 nM, and quantum dots in buffer solution at 6.38 µM. It was also proven that phosphor dots could be detected to a concentration of 23.10 µM. The Fire I lens-less CCD was able to detect C-reactive protein (CRP) with a LOD of 5.65 µM which is just above the “normal” clinical range 3- 5 µM.

Having proven that the lens-less CCD can detect fluorophores so near to clinical values for C - reactive protein (CRP), a proof of concept Hand Held Biological Lens-

less Detector (HBLD) was designed and built to show how it could be used in a Point-of-Care/Lab-on-Chip (POC/ LOC) application.

A custom iPhone application was created to connect to a central data base in order to provide up-to-date and accurate results and to control and monitor the progress of the C-reactive protein/Lab-on-Chip test being performed. The Hand-held Biological Lens-less Detector (HBLD) was also connected to a central server, which upon completion of a C-reactive protein (CRP) test, interpreted the test results, generated a custom, patient-specific report in PDF format, and sent to either a text message or an e-mail. A custom server program also sent the results to a smartphone so that the results could be reviewed.

Through this experimental study it was found that indeed a lens-less charge-couple device (CCD) can be used for the detection of organic and inorganic fluorophores. Furthermore, this device can be miniaturized into an effective, hand-held Point-of-Care (POC) microfluidic Lab-on-Chip (LOC) detector.

To be an effective POC device, a detector needs to be connected in some way to a central database to provide up to date and accurate results. To display the results a custom iPhone application (App) was created to control and monitor the progress of CRP LOC test that is being performed. The HBLD is wirelessly connected via a router to a smartphone, such as an iPhone. The HBLD is also connected to a central server that upon completion of a CRP test interprets the test results and generates a custom patient specific report in PDF form and sends either a text message or an email. A custom server program also sends the results to the iPhone so that the results can be reviewed.

## ACKNOWLEDGMENTS

First and foremost I am indebted to my mother Sandra Morra for all of her help support, and encouragement in this endeavor. I would like to thank my advisor, Dr. Mohammad Faghri, whose encouragement and guidance has allowed me to investigate such an emerging technology as microfluidic devices. Dr. Faghri has created a unique research group "on the cutting edge of the technology" known as microfluidics. I would like to thank him for introducing me to the field of microfluidics and allowing me to make contributions to this field.

This research project could not have been realized without the valuable input of Dr. Constantine N. Anagnostopoulos. His expertise in electrical engineering, specifically in CCD imaging, was crucial in determining the direction for this project.

I am indebted to my committee members Dr. Musa Jouaneh, Dr. Zongquin Zhang, Dr. Geoffrey D. Bothun, and Dr. Keykavous Parang for taking the time to be a part of my doctoral experience.

This endeavor would not have been possible without the help of my colleague Nicholas DiFilippo. His dedication and hard work was essential in the success of this research project.

I would also like to thank my other group members Dr. Peng Li, Dr. Toru Yamada, Mike Franzblau, Mike Godfrin, Jeremy Cogswell, Andrew Marchesseault, Mark DiFilippo, Leudi Mena, Carlos Javier and Ryan Andrews for all the help and support that they provided.

Finally, many thanks to David Ferreira in the machine shop. His skills and expertise were extremely helpful in the fabrication of the components of the hand-held device as well as the LOC molds.

## TABLE OF CONTENTS

## LIST OF TABLES

## LIST OF FIGURES

## NOMENCLATURE

| | |
|---|---|
| AC | Alternating Current |
| ADC | Analog to digital converter |
| App | Smartphone application |
| BBA | biobarcode amplification |
| bit | Binary digit |
| BSA | Bovine Serum Albumin |
| CCD | Charge-coupled device |
| CdSe | Cadmium selenide |
| CdTe | Cadmium telluride |
| CMOS | Complementary metal-oxide semiconductor |
| CNC | Computer Numerically Controlled |
| CRP | C-reactive protein |
| DC | Direct Current |
| DHCP | Dynamic host configuration protocol |
| EEPROM | Electrically Erasable Programmable Read-Only Memory |
| ELISA | Enzyme-linked immunosorbent assay |
| FDA | U.S. Food and Drug Administration |
| FITC | Fluorescein Isothiocyanate |
| FWHM | Full width half maximum |
| GUI | Graphics user interface |
| HBLD | Hand-held biological lens-less detector |

| | |
|---|---|
| HRP | Horseradish Peroxidase |
| HTTP | Hypertext transfer protocol |
| JPEG | Image format with lossy compression |
| LASER | Light amplification by stimulated emission of radiation |
| LFA | Lateral flow assay |
| LED | Light emitting diode |
| LOC | Lab-on-Chip |
| LOD | Limit of Detection |
| MB | Megabyte |
| MC | Microcantiliver |
| MISO | Master in slave out |
| MMR | Microring resonator |
| MOSI | Master out slave in |
| Mps | Megabytes per second |
| NA | Numerical aperture |
| NW | Nanowire |
| OFM | Opto-fluidic microscope |
| OLED | Organic light emitting diode |
| PBS | Phosphate buffered saline |
| PCB | Printed circuit board |
| PD | Photodiode |
| PDMS | Polydimethylsiloxane |
| PEG | Polyethylene glycol |

| | |
|---|---|
| PMT | Photomultiplier tube |
| PNG | Portable network graphics |
| POC | Point-of-Care |
| PWM | Pulse width modulation |
| PVDF | Polyvinylidene difluoride |
| RAW | Image format with minimal processed data |
| RGB | Red, Green and Blue Image |
| ROI | Region of Interest |
| SEB | Staphylococcal enterotoxin B |
| SCL | System clock line |
| SCK | System clock |
| SMTP | Simple mail transfer protocol |
| SMR | Suspended microchannel resonator |
| SHMP | Simple network management protocol |
| SNR | Signal to Noise Ratio |
| SPI | Serial peripheral interface |
| SPR | Surface plasma resonance |
| SS | Slave Select |
| STD | Standard deviation |
| TCP/IP | Transmission control protocol and internet protocol |
| TFTP | Trivial file transfer protocol |
| TIFF | Tagged image file format |
| TIR | Total internal reflection |

| | |
|---|---|
| Qdots | Quantum dots |
| UART | Universal asynchronous receiver/transmitter |
| UDP | User datagram protocol |
| U.V. | Ultraviolet |
| VGA | Video Graphics Array |
| WEP | Wired equivalent privacy |
| Wi-Fi | Wireless (Radio waves) |
| ZnS | Zinc sulfide |

# CHAPTER 1

## INTRODUCTION

Point-of-Care (POC) testing is a fast growing area in the field of clinical diagnostics. The POC market allows for the decentralization of clinical laboratories and allows for onsite patient care. Hand-held blood glucose meters are the most familiar type of POC devices on the market today. The glucometer has made a significant impact on global health care due to its reliability, efficacy, cost effectiveness and overall availability.

Lateral-flow-assay POC devices are the most common for the detection of proteins however, they are not quantitative in their results. An example of this limitation is a pregnancy test strip which indicates that a woman is pregnant but not for how long she has been pregnant. Some protein test require that quantitative results be known, such as in the case of cardiac bio-markers. Normal or abnormal levels of cardiac enzymes are crucial in determining a patient's diagnosis.

This dissertation introduces a new approach for a detection device to be used in a hand-held Point-of-Care microfluidic Lab-on-Chip (LOC) biological detection device (HBLD). The quantitative detection of fluorophores is necessary for an accurate POC device. The uses of microfluidic LOC technologies have allowed the miniaturization of standard laboratory equipment and help reduce the time necessary to achieve an accurate result. The focus of this dissertation is placed on detection with the charge-coupled device (CCD) imager and several areas that need to be improved upon in order to achieve a viable POC device. With significant advancements being

made in the area of optical detection devices, some of these advancements were employed into a POC device to make a truly hand-held unit. The use of a CCD similar to a webcam is the primary detector. One significant advantage of using CCD devices is that they are inexpensive and easily adaptable to a variety of applications. CCD imagers can be used in an LOC with reader or a POC device containing the reader. Removing the lens from the CCD device dramatically reduces the overall size of the detection device for use in a POC detector. A new way of interpreting the signal was devised to maximize the signal emanating from the detection site.

Current POC devices in the area of study (microfluidics) are still relatively large, not easily transportable and not interconnected to provide current patient information. These devices also require large amounts of samples and reagents and often need to be operated by highly trained health care personnel. For all of these reasons a hand-held POC LOC detection device for the detection of a biological biomarker, such as C-reactive protein (CRP), was designed and built. The Hand-held Biological Lens-less Detector (HBLD) detection device is part of a total system that is connected wirelessly to a smartphone device. A custom iPhone application (App) was created to control as well as monitor the progress of the test being performed. This App will allow the user to have easy access to up to date information and to be confident that the results will be properly recorded. The HBLD is wirelessly connected to a central server that can interpret the test results and generate a custom report in PDF format.

## 1.1 Optical Detection

### 1.1.1 Optical Detector

A light detector converts incoming optical energy into electrical signals and is the device used to capture an image. The two main types of optical detectors are photon detectors and thermal detectors. Photon or light detectors produce electrons from incoming photons. The electrons are then detected by the electronic circuitry and converted into a digital signal. Some thermal detectors convert the optical energy to heat energy which then generates an electrical signal or changes in the electrical resistance. Most photonic applications rely on optical detectors for measuring incoming light energy. This dissertation though, will focus only on the use of photon optical detectors.

Optical detectors, often called "square-law detectors", respond to power that is proportional to the square of the electric field associated with the electromagnetic wave. Optical detectors can be classified into three categories: photoconductive, photovoltaic and photoemissive [1]. Photoconductive detectors produce free electrons from incoming light which changes the conductive characteristics of the detector's material. This change in electrical conductivity can be measured and is a representation of the change in intensity of the incident light. The second type of detector, known as photovoltaic, contains a junction between two semiconductor materials and the change in conductivity is due to the presence of electrons in the junction region. When optical energy strikes the device a voltage is generated and can also be measured. The final type of detector, photoemissive, is based on incident photons releasing electrons from the surface of the detector material. When a

photoconductive material is connected in a circuit it acts a resistor or photoresistor, and the photoresistor resistance decreases with increased light intensity. This research will focus on the photoconductive type of detector known as a Charge-Coupled Device (CCD).

Currently there are two main optical imagers: one is the CCD and the other is the Complementary Metal-Oxide Semiconductor (CMOS). CMOS sensors are inexpensive, consume very little energy and have stable outputs. However, CCD's have better sensitivity to light, larger geometric fill factors, and lower associated noise. For these reasons CCD's were chosen as the detectors for this research [2].

A CCD is a silicon based integrated circuit made up of a dense matrix of detectors or pixels ( See Figure 1 &2). The CCD was originally invented by researchers at Bell laboratories as a memory circuit. However, its photo interaction with light made it much more useful. A CCD operates by converting light energy (photons) into an electronic charge. The interaction of photons with silicon atoms near the surface generates electrons. These electrons are stored in potential wells directly below the surface and are periodically transferred to a CCD shift register and each pixel is read out by a single on-chip, low noise amplifier one at a time (Figure 1).

The output from a CCD is in the form of analog signals. These analog signals are converted to a digital signal by the use of an analog-to-digital (A/D) converter, or ADC. This ADC converts the analog output of the sensor to a sequence of integer numerical values [3]. Depending on the density and size of the CCD device the ADC creates equally spaced horizontal and vertical boxes or scan lines (Figure 2).

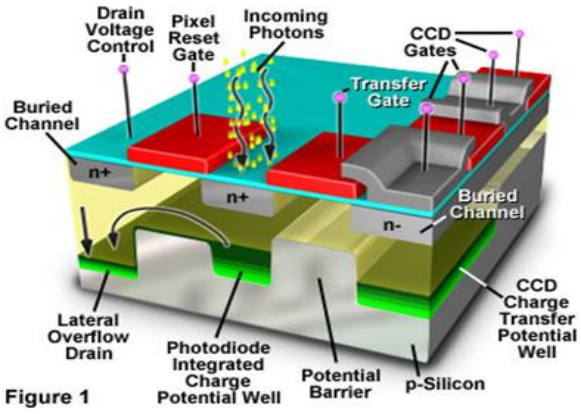


Image courtesy of Hamamatsu.

**Figure 1. Descritption of a charge-coupled device (CCD)**

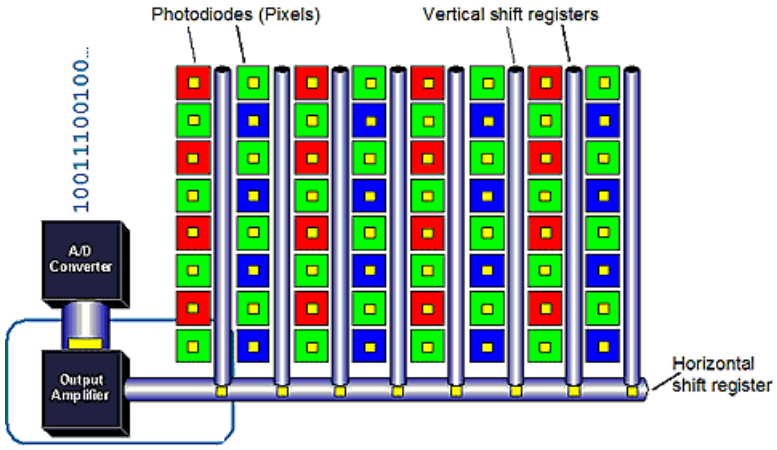


**Figure 2. Top View of CCD device with ADC controller**

The ADC then subdivides each scan line into a discrete number of units with a 4:3 ratio of horizontal pixels to vertical pixels. An example of this would be a 1.3 Mega pixel CCD device which has a 640 x 480 pixel density. The analog voltage must be sampled frequently enough in time and amplitude (or brightness) to produce a numerical reproduction of the signal. The numerical values that are obtained represent the intensity or brightness of the optical image that is observed averaged over a time

period and is called a pixel value. Each pixel value is denoted by three numbers. The first two numbers represent the x and y location, and the third number represents the signal amplitude. The amplitude ranges from a value of 0 to 255 for an 8 bit color system. Thus, an imager file, representing the image, consists of an array of numbers, containing the location of each pixel and the value of the signal intensity at that location (Figure 3).

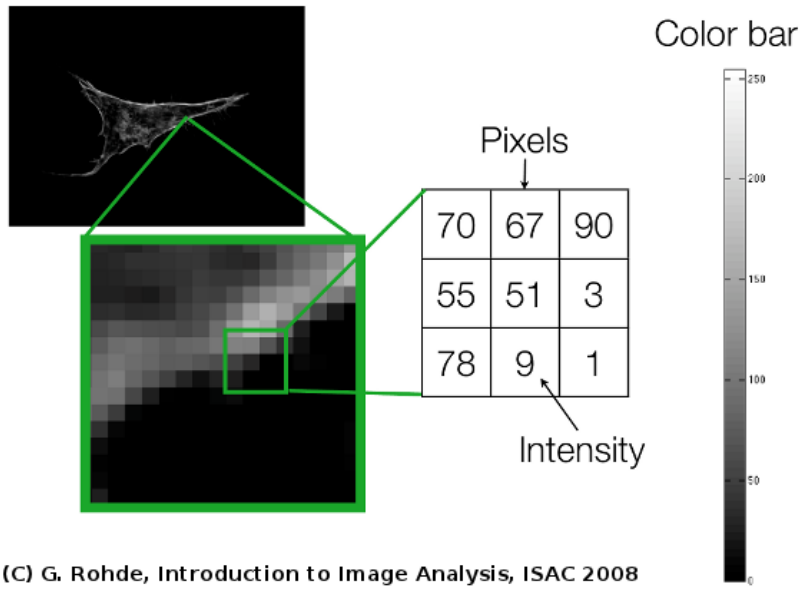


**Figure 3. Zoomed in view showing individual pixel values and its corresponding Color map (8 Bit)**

The number of bits used to indicate the color of a single pixel is known as the bit depth or color depth. The more bits that are used, the finer the color levels that can be represented. Black and white images (monochrome) are known as 1 bit color depth and the integer values range from 0 to 1. The most common color depth is the 8 bit, and it has an integer range from 0 to 255. A color bar or map which represents color

depth per bit can be seen in the above (Figure 3) where higher numbers represent higher brightness values of each pixel. As computing power and memory increase, the ability to integrate higher level color depths also increases. Currently there are 24 bit, 30 bit, 36 bit and 48 bit color depths; however the 48 bit has $2^{48}$ values which is a range from 0 to 2.81e14 bits per pixel. This is very important, because one could actually have more data than necessary. The more data that is acquired the more computational time is required. Also, more data means more memory, which increases the cost of the computational hardware.

The surface of the CCD imager has a color filter array placed on top of the individual pixels. This color array pattern is known as a Bayer pattern and consists of alternating red, green, and blue filters. Each pixel can be thought of as a tiny cup into which photons will fall. The filter array separates the colors and then the pixel reads the brightness values (Figure 4). The Bayer pattern has twice as many green pixels than red or blue. This is an attempt to match the human eye is able to distinguish shades of green better than any other color.

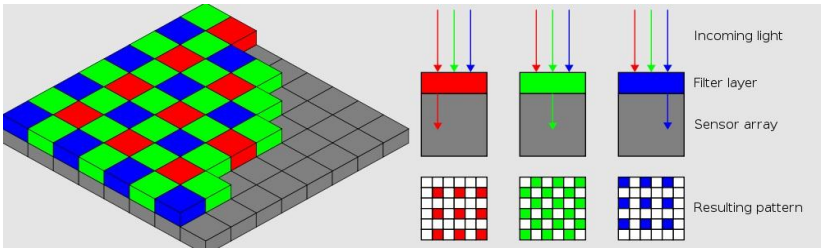


**Figure 4. Bayer pattern on CCD imager shown with with either red,green or blue filter on top of each individual pixel**

### 1.1.2 Digital Image Format

The type of digital image employed depends upon its intended use. Three of the most common formats that are used to store digital representations are Joint Photographic Experts Group (JPEG), Tagged Image Format File (TIFF) and unprocessed data (RAW). Most digital image formats have some type of image compression to reduce the overall memory required to store the digital representation. Image file compression is a process where a complex computer algorithm reduces the number of redundant pixel signals. JPEG is the most commonly used digital image format. The main reason that the JPEG file format is popular is due to its ability to store good quality images while minimizing the overall file size. The JPEG image format compresses some of the digital image with a method commonly referred to as a "lossy" format. The lossy method is capable of producing a much smaller compressed file while providing enough information to recreate the original image. The main disadvantage of the JPEG file format is that it suffers from a generation loss whereby it progressively loses some of its quality due to the lossy compression. As a result every time the image is viewed or stored it losses some more data and this data cannot be recovered. TIFF is considered to be one of best file formats for managing exquisitely detailed images without losing most of the details that would be lost in a normal compression scheme. The TIFF file format is ideal for editing digital images due to the large amount of original information. However, the best quality image format is RAW. RAW is a non-compressed representation of the original image, therefore the pixel values are the true value that the CCD imager generates. The RAW format is equivalent to a digital "negative". Since there is no data loss due to

compression, the RAW format can easily be converted into other formats like TIFF or JPEG. The RAW data can also be changed somewhat to reflect color balance, contrast and density before being converted into other file formats (Figure 5). The major disadvantage of the RAW format is the size of the image files. For the purpose of this research project the RAW data will be the file format used because there is no compression of the data.

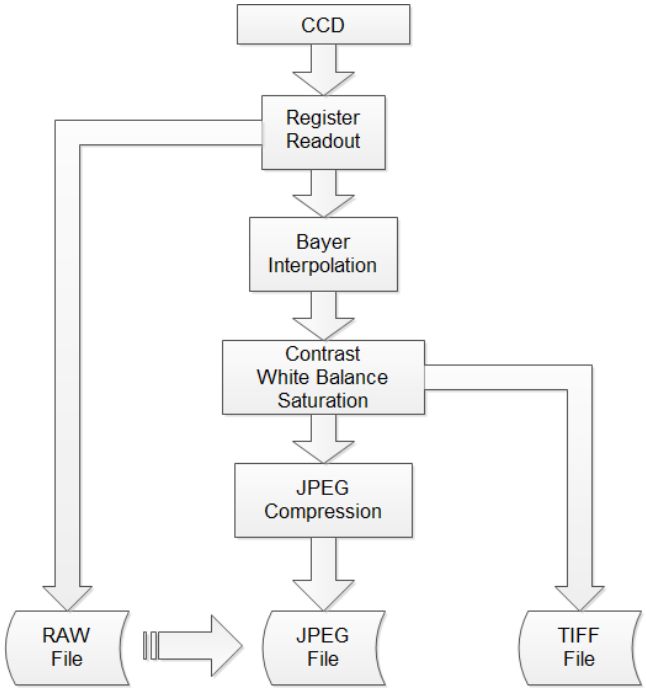


**Figure 5. Flowchart representing the path of the CCD data to its final file conversion**

## 1.2 Fluorescence Spectroscopy

Fluorescence is a process in which a material emits light when it transfers from an electronically excited state to a ground state. These electronically excited states are created by a mechanical, chemical or a physical action. A partial energy level diagram is shown in Figure 6.

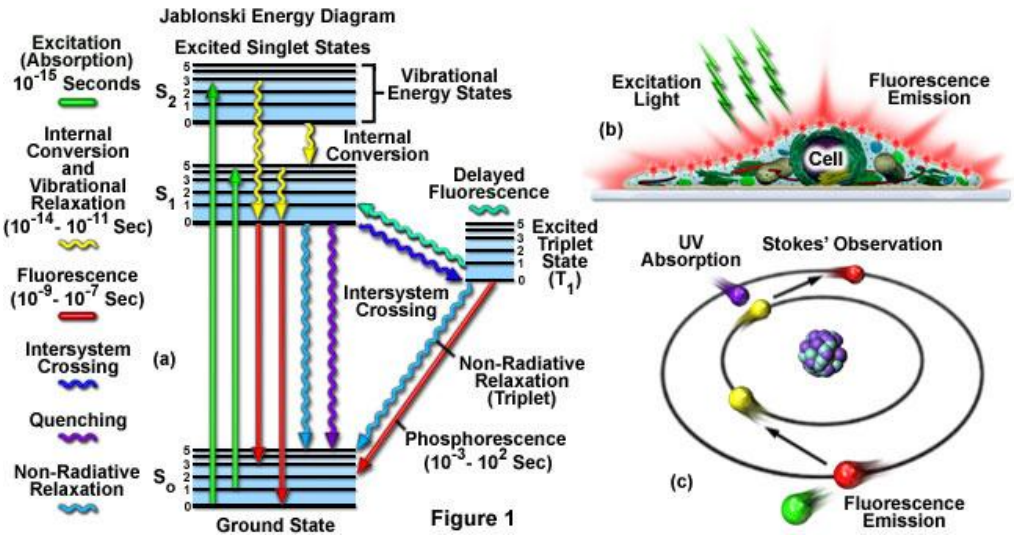


**Figure 6. Fundamental concepts of fluorescence microscopy**

A photo luminescence molecule is usually divided into two categories, fluorescence and phosphorescence. Fluorescence is the process by which a molecule or atom absorbs light at a particular wavelength (excitation wavelength) and after a certain amount of time it emits a longer wavelength of lower energy (emission

wavelength). Phosphorescence is similar to fluorescence but has a longer interval between the excitation and the emission.

A technique known as fluorescence microscopy has become an extraordinarily useful tool in the field of the life sciences. It is extremely powerful when used for the staining of biological molecules, examining the dynamics of protein, protein interactions and immunofluorescence assays. The research project is based on the fluorescence imaging method of biological detection. An example of a fluorescence microscope is shown in Figure 7.

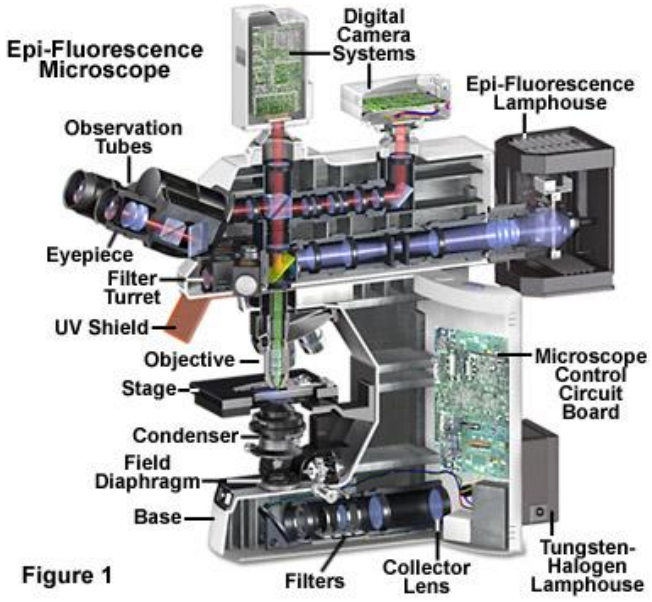


**Figure 7. Epi Flourescence Microscope**

All fluorescence instruments contain some basic items: light source, sample holder, filter, dichroic mirror and detector. Understanding each component is crucial to the development of a POC device. The most common sources in fluorescence spectrometry have spectral outputs that are either as a line source or a wide spectrum of light. These light sources include arc Xenon lamps, high pressure Mercury lamps,

Quartz- Tungsten lamps, LEDs and laser diodes among others. Every type of light source has advantages and disadvantages and proper selection is necessary to provide the best results. The major difficulty of implementing a light source is that these sources usually require large amounts of energy are delicate and are extremely expensive. This research focused on two inexpensive and compact light sources, LED and laser diode.

Recent advances in microfluidic technology have allowed researchers the ability to alter the normal biological sample holder of a microplate. The use of polymers such as Polydimethylsiloxane (PDMS) has allowed endless styles of sample holders that can be custom designed for any specific application.

A fluorescence microscope is only as good as the filters that are used. Most fluorescence microscopes use a combination of excitation filters, a dichroic mirror and an emission filter. Combining these filters in the correct sequence allows the user to select only the correct wavelength of light for each specific fluorophore. The excitation filter allows only a select range of wavelengths to excite the sample. An Epi-fluorescence microscope uses a special filter/mirror called a dichroic mirror. This dichroic mirror reflects the excitation light but allows the emission light to travel through to the emission filter and then to the detector. The emission filter ensures that the light hitting the detector contains the minimum amount of unwanted light. These filters are usually preset for specific fluorophores and will allow for the maximum signal with minimum noise. However these optical filters add significantly to the overall size of the detector. Incorporating all of these filters into a POC device is not

currently feasible, but selecting the correct excitation light sources and incorporating an emission filter into a design would allow for the optimum results.

A fluorescence detection instrument must have some type of optical detector. Depending on the method of fluorescence detection the detector could be an avalanche photodiode (APD), a photomultiplier tube (PMT), a CMOS, a CCD or others of the many available [4]. The single point optical detectors such as APDs and PMTs are extremely accurate. However they lack the ability to detect over a large area. PMT are large and expensive compared to other optical devices.

Fluorescence detectors may also have single and multiple channels for multiple fluorophore detections at the same time. Single channel detectors are more accurate but are very limited in wavelength detection and usually use some type of optical filter. Multiple channel detectors are superior for detecting many fluorophores [5]. For all of these reasons this research will focus on the single channel detector. The following is a discussion relevant to this part of the project.

One major advantage in using fluorescence microscopy is the vast number of fluorophores that are commercially available. Each has a unique excitation and emission characteristic. Each type of fluorophore has a specific quantum yield which is the efficiency of the energy transferred from incident light to emitted light.

Another important characteristic of fluorophores is the fluorescence lifetime, which is the time that a molecule emits light after the excitation light has hit the molecule and before the molecule decays to a ground state. Fluorophores such as fluorescein and its derivative fluorescein isothiocyanate (FITC), can be used for live cell imaging and provide an excellent contrast in microscopic imaging. Several

different molecules can be imaged simultaneously by using multiple fluorophores. An example of this is that multiple quantum dots with different sizes will emit different wavelengths using the same excitation light source. This multiple emission allows for multiplex detection schemes.

Quantum dots or Qdots are nano-sized semiconductor particles that can exhibit unique optical properties. One very desirable quality of Qdots is that they have a great resistance to photo bleaching which makes them extremely useful to live cell imaging and other fluorescence techniques. Qdots have an increased brightness when compared to other fluorophores which is particularly helpful in biomedical immunoassays. Most quantum dots are made of a center core that is only a few hundred to a few thousand atoms of Cadmium Telluride (CdTe) or Cadmium Selenide (CdSe). In order to improve the optical and physical properties of these Qdots, most manufacturers surround the Qdots with an outer shell of Zinc Sulfide (ZnS). Some Qdots have a polymer coating applied to the shell to provide a platform for bonding of the nanocrystal with biological reagents or antibodies. Most Qdots have a polyethylene glycol (PEG) linker which helps reduce the non-specific binding that can occur in many biological assays. The majorities of Qdots have a molecular weight of between 500 and 650 kDalton and have an average diameter of about 20 nM (Figure 8). Since the emission light is inversely proportional to the size of the Qdot, the smaller the Qdot, the higher the energy (ex. blue light), the larger the Qdot the lower the energy (ex. red light).

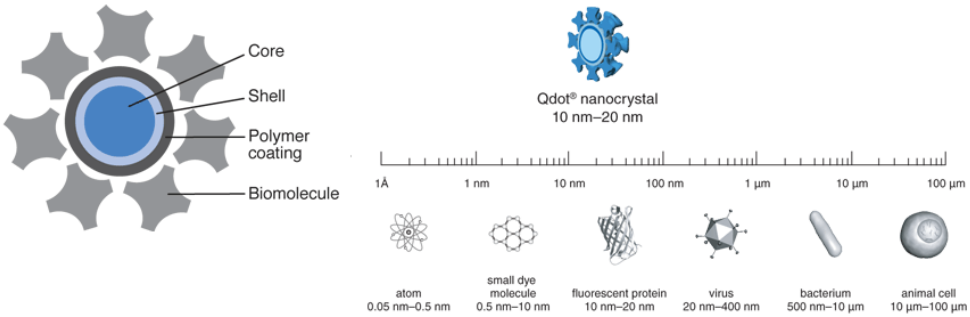


**Figure 8. Anatomy of a Quantum Dot and Relative Size**

Another type of fluorophore that has become more commonplace of late is the phosphor-based nano crystalline fluorophore commonly known as phosphor dots. Phosphor dots behave in a manner similar to quantum dots. The major advantage of using phosphor dots is that they are non-toxic. Phosphor dots are cheaper and have a longer life than quantum dots. They are becoming very popular for biomedical applications such as bioassays, in vitro imaging (outside the organism), in vivo imaging (inside the organism), and molecular tracking. Phosphor dots are also very soluble in water. This is important because most biological applications are in aqueous solutions. As a result, no chemical modifications to the detection surface are needed. Phosphor dots can also be used in multiplex assays due to the fact that they can have simultaneous excitation using the same UV light source. The three mentioned fluorophores FITC, Phosphor Dots and Qdots were investigated for use as a primary label for an immunofluorescence assay for this LOC POC device.

### 1.3 Lab-on-Chip Fabrication and Design

The development of microfluidic LOC devices for use in biochemical analysis has enjoyed a dramatic increase in recent decades. There are several methods of producing microfluidic channels such as hard lithography, soft lithography,

micromachining, embossing and laser etching. A substantial percentage of this growth is due to the use of an elastomer called PDMS which uses soft lithography fabrication techniques. This method of fabrication is much easier and more reliable than past methods of channel fabrication such as hard photolithography.

PDMS has the following characteristics: low cost, easy usage, easy fabrication, reliable feature retention, transparency and speedy fabrication [6, 7]. PDMS is easily bonded to itself and other silicon surfaces, such as glass, using standard plasma ashing techniques. PDMS also has a refractive index similar to that of glass. Its properties of transparency and non-reactiveness and the fact that its mechanical properties remain constant over a wide variety of temperatures are what make PDMS an excellent fabrication material. The design of a pattern to be used can be accomplished via a variety of software, such as Solidworks or Adobe Illustrator. Fabrication of a PDMS chip is very easy and does not require expensive equipment to design intricate LOC devices. PDMS and soft lithography techniques were used in this project due to the ease of fabrication and reproducibility.

### 1.4 Point-of-Care Devices

The POC market which is currently valued at 13.8 billion dollars is expected to rise to 15.5 billion dollars by 2016, with the biggest area of growth in the area of blood chemistry testing [10]. The main reason that the POC market has become so relevant is because of two factors: enhanced portability and networking capabilities [11]. POC devices are commonly described as “decentralized” and “remote laboratory testing facilities” and have made a significant impact on patient care in developing

countries.[10, 11] A POC device needs to be as accurate as any laboratory test and easy to use. An effective POC device should securely share information about a patient's status. Most current LOC devices whether they are compact or portable need to be docked to transfer results. The ever-increasing number of Wi-Fi portals has allowed portable device users to transfer data securely across Wi-Fi networks. The Wi-Fi specification is a wireless extension of Ethernet that supports transmission control protocol and internet protocol (TCP/IP) and allows for wireless transmission speeds up to 54 megabits per second (Mbps) at distances of up to 1,000 feet [12]. Bluetooth technology is also a viable wireless portal for data communication. Bluetooth enables a device to use radio waves to transmit data and operate in the scientific and medical (ISM) band at 2.4 to 2.485 GHz for up to 50 meters [13]. Secured Wi-Fi portals allow POC devices to instantly update patient records from the POC device to ensure that a central database properly reflects the most current information. Bluetooth technology is also acceptable for shorter distances however it works at a speed 10 times slower than Wi-Fi. For this research project, and the development of the prototype device, Wi-Fi was used as the data transfer method.

CHAPTER 2

# REVIEW OF LITERATURE

## 2.1 Optical Background

In recent years the combination of optics and microfluidics has resulted in the miniaturization of traditional fluorescence microscopy [18]. The resulting optofluidics have brought about enhancements in detection techniques: such as absorbance, fluorescence and chemiluminescence [19]. However, optical microscopy has several limitations including a lack of portability, a high cost due to the use of expensive optics, and a need for regular maintenance. To overcome these limitations, lens-less and portable charge-coupled device (CCD)-based platforms have been recently developed [16, 17].

Most integrated imaging systems use less bulky and less expensive components, while improving detection limits. Recently a group of researchers from Stanford University developed a miniaturized integrated fluorescence microscope comprised of mass producible parts. The detection device is a CMOS imager coupled to a field programmable array used for high speed cellular imaging [18, 19]. This system uses a CMOS array with no attached lens but instead uses an achromatic lens and dichroic mirror in the final design. The Stanford researcher's device allowed them to focus in on the sub-micron level while using mostly inexpensive light sources and control systems. Even though this device is compact it must be connected by nine wires to an external PCB board to interface all the components to a computer.

The employment of a lens-less CCD for an image device for use in a bio-sensor is not a new concept. Researchers at Harvard Medical School in Boston, Massachusetts, mounted a microfluidic chip directly to the surface of a CCD to count the number of cells that passed from one end of the microfluidic chip to the other [14]. This method of cell counting was effective and quick, however, there was a considerable distance between the light source and the detection surface, which creates a larger imaging device. Furthermore, the light source that was used was an expensive, halogen white light.

In yet another effort, researchers at the University of California, Department of Electrical Engineering, demonstrated on-chip fluorescence detection using an ultra-large field of view, lens-less CCD sensor array [20]. This detection setup used the principle detection method of total internal reflection (TIR) for the detection of fluorescence labeled cells. This method of detection is very useful and is effective at separating the excitation light from the emission light through the use of a prism. In TIR, the excitation of the fluorophores is achieved through evanescent waves, which occur in the sample at levels that are only a few hundredths of microns thick. This means that samples need to be extremely thin in order to do a complete analysis. This system has some disadvantages when trying to implement it into a hand-held device. The excitation light is an expensive light source (Xenon light) and is also at a long distance from the chip. This method requires a substantial amount of time to complete one test (approximately 10 minutes per image). This particular lens-less detection method has the capability of detecting labeled white blood cells which are of the order of 7 -19 micrometers in diameter.

A lens-less wide field CCD was used by researchers at Brigham and Women's Hospital, Harvard Medical School, Boston, Massachusetts, for the detection of CD4 counts of HIV-infected patients [21]. The researchers using the lens-less CCD captured images representing the diffracted shadow signal of the tagged CD4 held by the anti CD4 antibodies which were present on the functionalized microfluidic chip. The system was battery-powered and could be designed into a POC device, but this system needs to be attached to a computer in order for the data to be transferred, and the imager does not return the RAW data.

A recent journal article called "Comparative Advantages of Mechanical Biosensors" published in Nature Nanotechnology compared the various types of mechanical biosensors for analysis time and LOD. Figure 9 shows the detection limits for the sensing of proteins versus the analysis time for nine types of detection methods. Figure 9 compares the following types of detection: (1) SPR- surface plasmon resonance, (2) SMR - suspended microchannel resonator, (3) NW - nanowire, (4) LFA – lateral flow assay, (5) MMR-microring resonator, (6) QCM – quartz crystal microbalance, (7) BBA – biobarcode amplification assay, (8) IFA - immunofluorescent assay, (9) MC – microcantiliver. Figure 9 also illustrates the present day state of the art capabilities. Some of these methods such as MC or MMR are extremely accurate but use large and expensive devices.

The two most common types of detection methods are lateral flow assay (LFA) and enzyme linked immunosorbent assay (ELISA). LFA's are easy to use, accurate and provide quick analysis time. However, their concentration sensitivity is not sensitive enough for most biological tests. ELISA tests have much better concentration

sensitivity but require substantially more analysis time [22]. The ideal detector is therefore able to provide timely and accurate results at a lower cost and shorter time.

The method that was focused on in this research was IFA, and a visual representation can be found in the brown oval in Figure 9. Previous POC devices by a University of Rhode Island colleague Peng Li created an IFA that uses a spectrometer for optical detection giving results found in the large green oval in Figure 9 (LOD 1.9 nM, 19 min) [23]. The best "state-of-the-art" results fall in the large grey triangular area. The results from this research are in the black oval, and will be very close to the line for present day "state-of-the-art" detection.

The goal of the research presented in this dissertation was to develop a lens-less CCD detector that is capable of achieving a lower LOD and a lower assay analysis time than that shown in the brown oval in Figure 9 and test results confirm that the results of the goal have been met.

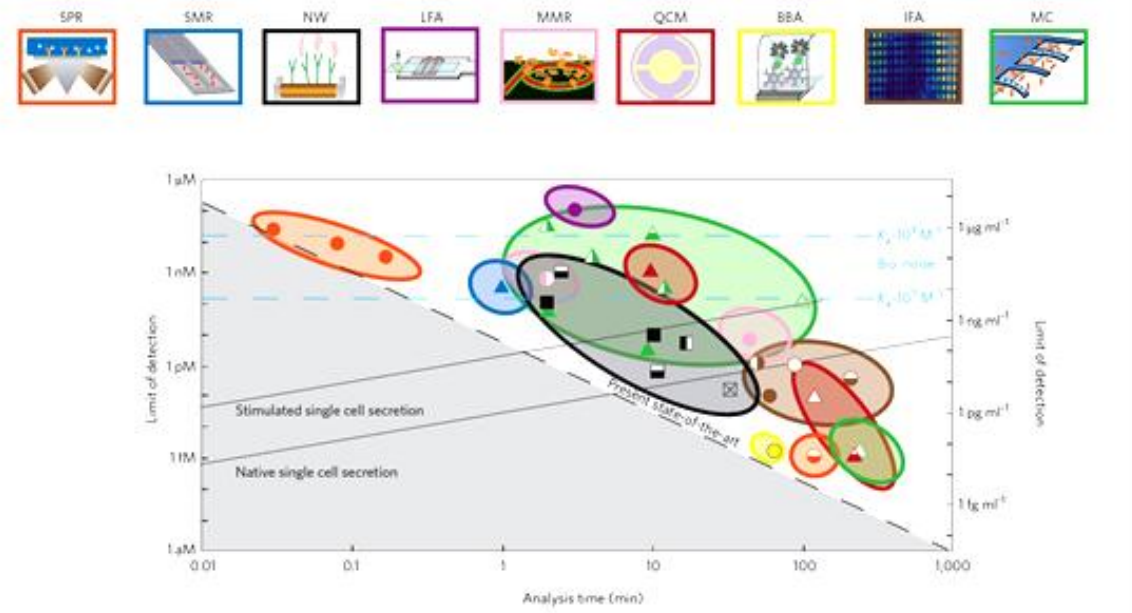


**Figure 9. Different methods of detection and their LOD vs. analysis time**

A recent article written by Gurkan from the Harvard Medical School in Boston, Massachusetts outlined emerging lens-less imaging technologies and concluded that the use of a CCD or a CMOS has significant advantages over other optical detectors [24]. Some of these advances cited were in the areas of cost, accuracy, flexibility of operation and functionality of the various optical detectors. The author indicated that one major advantage of a lens-less optical device is that the same optical detector can be designed for use in a resource limited POC device as well as conventional diagnostic device. The design of medical devices is an extremely costly endeavor and producing one design that could meet the needs of multiple end users and could drive down the cost of these diagnostic instruments is highly desirable [25].

## 2.2 POC Background

There is an ever-increasing need for an easy-to-use, disposable, fast, accurate and reliable Point-of-Care (POC) diagnostic and Real-time monitoring system [26, 27]. In resource-limited settings, a microfluidic device could have a dramatic impact on the detection of infectious diseases on a global level [14]. Recently, microfluidic devices have become attractive due to their low cost, small sample size and fast results. Having a hand-held diagnostic device that can deliver on-site results could be crucial in providing accurate and timely diagnosis [28].

The current POC market is largely dominated by products based on lateral-flow assays (LFAs) that are typically fast, but provide only a binary indication of health status (e.g., home pregnancy urine test strip) [19]. In addition, LFAs frequently display limited sensitivity and sometimes limited specificity [29]. Rapid and affordable POC diagnoses with superior sensitivity are urgently needed in many

scenarios of our society from home health care and environment monitoring to disease outbreaks and biodefense. However, most of the critical diagnostic tests are still conducted in sophisticated clinical or reference laboratories with enzyme-linked immunosorbent assay (ELISA) by highly trained personnel. Although ELISA provides a quantitative, specific, and sensitive detection approach for analyzing biological agents, it requires long incubation time (> 12 h) and multi-step fluid handling, which are impediments to immediate health assessment at the POC.

Over the past 15 years, microfluidic-based devices have demonstrated many attractive characteristics for analysis such as: fast turn-around time, low consumption of reagents, complex fluid handling, increased automation, capability for multiplexed tests, and miniaturization of the system. These unique features make microfluidics a natural fit for POC diagnostic devices.

There are currently two approaches to POC testing: pure disposables and disposables with a reader [30]. Similar to LFAs, which have been very successful in POC diagnosis, the disposable microfluidic-based diagnostic device requires only a disposable component and no external reusable instrument for operation. Such devices lend themselves well to applications such as qualitative or semi-quantitative assays in extremely low-resource settings. Several microfluidic disposable diagnostic devices have been developed for some very interesting applications such as the ABO Card (Micronics) for blood typing and the H-Filter (Micronics) for blood plasma separation [31]. The “disposable with a reader” model could be a more promising approach as it allows high performance with low per-test cost.

In recent years, POC devices incorporating reusable sensors and disposable cartridges have been developed and marketed. One such device is the Abbott i-STAT electrochemical blood analyzer [32]. The hand-held analyzer rapidly measures levels of electrolytes ($Na^+$, $K^+$, $Cl^-$, $Ca^{2+}$), general chemistries (pH, urea, glucose), blood gases (pCO2, pO), and hematology (hematocrit) with a disposable microfluidic cartridge. The Biosite has developed a POC device, named Triage Cardiac Panel, to aid in the diagnosis of acute myocardial infarction [33]. The device integrates a portable, battery-powered fluorometer with a disposable cartridge. Three cardiac markers from whole blood samples can be tested simultaneously in approximately 15 minutes. In May 2009, the US Food and Drug Administration (FDA) issued a Class I recall of the Triage Cardiac Panels because of the risk that they would produce a false negative test result [34]. Learning from these earlier achievements and limitations, it is necessary today to develop additional microfluidic-based "disposable with a reader" systems that have better performance than existing POC devices and that are geared to more bio-relevant applications. Thus, it comes as no surprise that many such efforts have been undertaken by many institutions and corporations on a worldwide scope.

C.H. AHN et al [6] presented an inexpensive, hand-held, disposable, self-contained immunoassay cassette for detecting antibodies to HIV in saliva samples. The cassette integrated four air pouches, a metering chamber, reagents storage chambers, a zigzag mixer, and a lateral flow strip into a polycarbonate microfluidic chip. The two salient features of this device were (1) using a timer-actuator for automated pumping and (2) up-converting phosphor particles for detection. To obtain

quantitative information from the assay, the lateral flow strip had to be removed from the cassette and read by an external fluorescence reader.

The Commonwealth Scientific and Industrial Research Organization in Australia developed a fully self-contained, hand-held biosensor based on the surface plasmon resonance technique [35]. Optical elements including a diode laser, a lens, a prism, and an array of photodiodes were successfully assembled into the hand-held unit along with the electronics. Reagent loading was achieved manually through a plastic cylindrical sensor cell and long incubation times were still needed. This system demonstrated label-free detection of ricin down to a level of 200 ng/mL by measuring the change in the refractive index.

Very recently, the Bio & Health Group of Samsung Advanced Institute of Technology in South Korea developed a portable, disc-based, and fully automated enzyme-linked immunosorbent assay (ELISA) system to test Hepatitis B virus from whole blood [36]. The device was comprised of a disc loader, a disc positioning and rotation controller, a laser position controller, an optical detection unit, a temperature controller and a user interface controller. The test could be completed within 30 min and the LOD was as good as that of the conventional ELISA. To achieve fluidic control, a diode laser was needed to induce phase transition of the Ferro wax micro valves.

From the above examples, it can be seen that the research on microfluidic-based POC devices has cut across many major disciplines including engineering (mechanical, electrical, and biomedical), biology, chemistry, and physics. Successful development and commercialization of a device requires effective collaboration

among academic researchers, industry, and clinicians. To facilitate such efforts, several competitive and coherent consortia have been established. The Bill & Melinda Gates Foundation is supporting a consortium (University of Washington, PATH, Nanogen, Micronics, and Invetech) to develop a multifunctional microfluidic device for near-patient diagnosis [26]. A conceptual model named "DxBox" was proposed and is currently under development. This hand-held DxBox will be able to combine polymerase chain reaction (PCR) and immunoassay. It will accept a finger-prick blood sample and will automate all steps within a disposable microfluidic cartridge.

As another example of such a consortium, sixteen partners from eight different countries across Europe are working together on the development of a POC system [37]. The aimed system named "the SmartBioPhone$^{TM}$" consists of a hand-held base unit (smartphone and reader) and a disposable lab-on-chip. This device will be fast, minimally invasive, and compatible with actual raw samples. It is aimed at four POC applications: environment, food, cancer, and drug monitoring. One draw-back may be that the sample must be injected into the LOC.

Currently there are some commercial POC LOC devices using lateral-flow immunoassays that are available which include the Afinion CRP detector [38]. The Afinion CRP detector is very accurate and somewhat simple to use. However, it requires that the diagnostic chip be refrigerated to 8 degrees C and chips have a short shelf life of about 6 weeks. Other commercial devices presently on the market require some form of manual manipulation of the LOC be performed to activate the bio-reagents, or they require that a large sample be injected into the LOC [32]. These

devices use a passive style of fluid flow as compared to an active one which uses a pump or a vacuum system [39].

A collaborative group of researchers from Harvard Medical School and MIT recently has demonstrated the feasibility of using a cell phone to facilitate microchip ELISA based non-invasive detection of a biomarker in urine [40]. The sample is loaded into a stamp-sized microchip that performs an ELISA analysis using horseradish peroxidase (HRP). The Smartphone, with a built in camera and a custom Smartphone application, is mounted onto an adapter that locates the Smartphone directly above a LOC, where images of the resulting sandwich assay are acquired. The images are then downloaded to a computer running MATLAB for pixel analysis. This method proves the concept of using a CCD from a Smartphone for the detection of a biological reagent on a microfluidic LOC. This system however, requires a significant amount of user input to complete the ELISA assay.

Despite these great efforts and with the notable exception of glucose sensors used by diabetic patients, there is no device that can offer "The Holy Grail" of a hand-held, easy to use, self-calibrating, automated, and inexpensive device that is capable of performing reliably fast, specific, sensitive, and quantitative tests for biomolecules using minimal raw samples.

# CHAPTER 3

# METHODOLOGY

The goal of this research was to develop a novel fluorescence portable hand-held lab-on-chip point-of-care biological diagnostic device. This detection device has been used for standard sandwich (ELISA) immunoassay tests. The inspiration of this new method of detection comes from a previously built shoebox LOC POC diagnostic device that was able to detect CRP in PBS buffer; but the onboard spectrometer was bulky and implementation was difficult. The methodology and procedures for investigating an optical detector for use in a portable hand-held LOC POC device involves research in the following five main areas:

1. Optical Detection
2. Fluid Handling
3. Wireless and iPhone Integration
4. Assay Protocol
5. Hand-held Reader Box

### 3.1 Optical Detection

POC LOC devices require a method of detection that is accurate, low cost, extremely sensitive and very compact. The system that this research focused on was based on a commercially available charge-coupled-device (CCD) similar to a webcam. The lens from the webcam was removed to allow for a more compact design. The use of CCD's as imagers is not new to microfluidic detection, but the method of its application has been changed significantly to reduce the space necessary for its implementation.

The detection system is based on standardized fluorescence imaging techniques, with a light source that is used to excite the fluorophores and the detector which is a modified CCD imager used to record the image. An illustration of this can be seen in Figure 10.

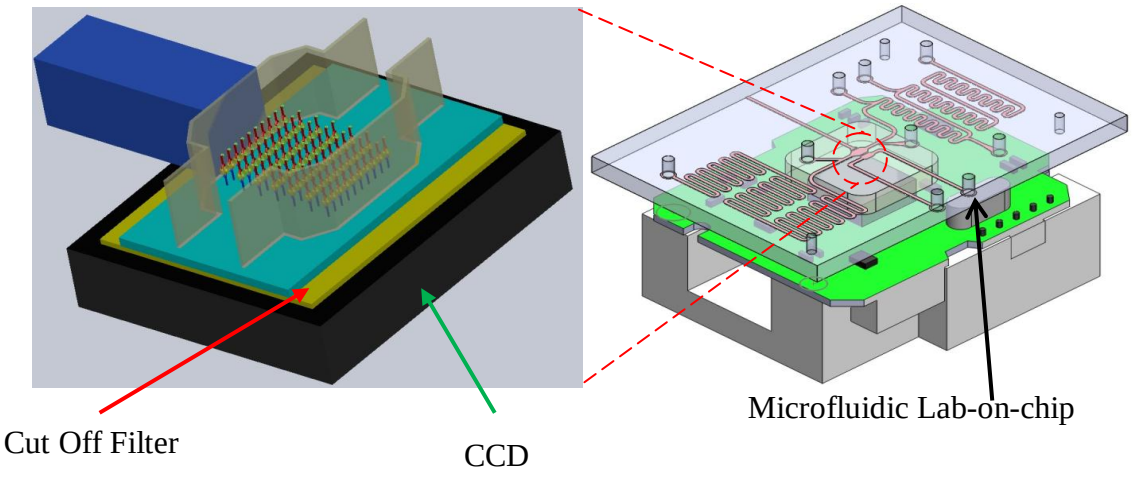


**Figure 10. Illustration of microfluidic chip with CCD mounted directly below the detection site**

For fluorescence detection there are optical filters that are designed to be used in conjunction with each type of fluorophore. Different filters were tested to optimize the signal. These filters were positioned between the CCD camera and the bottom of the detection chamber as shown in Figure 10. The investigation of these filters will be discussed later on in this chapter.

The quality of a digital image is usually determined by two factors. The first factor is often referred to as image resolution, and it is determined by number of pixels (pixel density) and range of brightness values associated with each pixel used in the image. A 0.3 Megapixel CCD has a 640 x 480 field of pixels. Increasing the number of pixels to a 3.1 Megapixel camera will increase the total pixel field to 2048 x 1536 and the higher the pixel density the higher the resolution. The second factor that increases the resolution is the positioning of the lens on top of the CCD device. Just like a normal camera, the accuracy of the image can be dramatically altered by changing the lens, however changing the lens is usually associated with focusing on a certain area of concentration. The new methodology for detection no longer requires focusing on one area. When the lens is removed, the CCD device can be placed directly in contact with the micro channel detection site or a cutoff filter located directly underneath the detection site. This method allows all the incoming light to be detected.

Most CCD's output a modified and compressed image, we used instead a camera that outputs the RAW data or data that is not preprocessed is used. Once the RAW data is returned, a true value of the emission light from the quantum dots can be detected and analyzed. Unlike normal image processing, this method of detection is

not concentrating on the actual image that is acquired. It is only concerned with each individual pixel value. The Bayer pattern on the CCD separates the different wavelengths of light and creates a matrix for each color that represents the brightness value present at a pixel. Therefore, three matrices are created: one for red, one for green, and one for blue. These matrices however, have voids due to the data interpolation that occurs in order to smooth out the visual recreated image. For the type of analysis that will be performed only the true non-interpolated values are desirable (Figure 11).

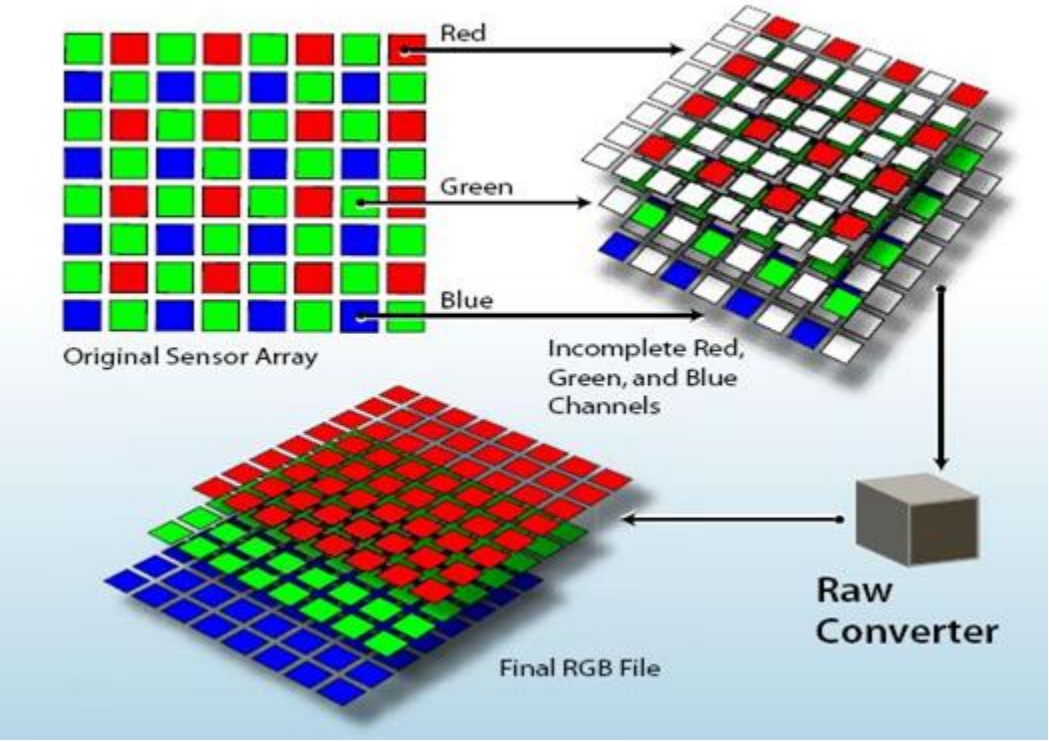


**Figure 11. Illustration of real data from CCD and the modified data that the onboard video driver delivers**

As indicated previously, only the pixel values with the color that corresponds to the emission wavelengths are analyzed. An important aspect in any digital CCD imager is the determination of the noise. The amount of noise can dramatically affect the accuracy of an image. The amount of noise compared to the signal is an important variable known as the signal to noise ratio (SNR). The SNR is a universal ratio used for many different applications, so defining the signal will determine how to use the SNR. For this application, the SNR is a comparison of the measured light signal to the total combined noise. There are two basic types of noise, spatial and temporal. Spatial noise is noise created due to the sensor design, and temporal noise is random noise created each time an image is captured [40, 41]. The temporal noise can be reduced by signal averaging, where N is the pixel value for each image captured.

$$N_T = \frac{\sum N}{N} \tag{1}$$

Since the temporal noise is an independent variable, the noise power not the voltage or pixel level is summed. Knowing that the voltage is proportional to the square root of power, the noise pixel level (which is proportional to noise voltage) increases by sqrt (*N*).

$$SNR = \sqrt{\text{Number of Images}} \tag{2}$$

This equation shows that as the number of images goes up so does the SNR. A compromise of the number of images captured to maximize the SNR while retaining minimal data was done by plotting a graph of SNR vs. Images. A series of test images was taken and the pixel intensities were averaged. Using a scaling factor of 100, it was determined that the SNR reached a peak value at N (number of images) equal to 10. After some initial baseline tests it was concluded that the CCD needed to take several images to "settle" the pixel value; that value is 2 images. Therefore 2 initial images plus the 10 to maximize the SNR comprise the 12 images taken for each sample and then twelve images are averaged to get a single value.

### 3.1.1 Optical Detection Setup

Initially the optical detection device was planned to be a dismantled Logitech C250 webcam with the lens removed. This webcam was chosen for its inexpensive and compact design. The Logitech C250 CCD imager is a 2.1 Megapixel imager that returns a standard RGB 8bit image. Figure 12 show the various stage of the initial prototype CCD imager. The original design used a commercially available Logitech C250 webcam that was disassembled and the focusing lens was removed. Figure 12 B shows the test stand that was rapid prototyped to securely hold the webcam for accurate alignment. Figure 12 C shows the wiring modifications to the Logitech webcam that were done to try to capture the RAW data [43]. The circuit modifications that were made included severing the connection between the ADC and the video processor and then bypassing the video chip. After some initial baseline testing for

noise, it was determined that this detection device with the alterations was too noisy. The noise levels were at least 10% of the pixel values.

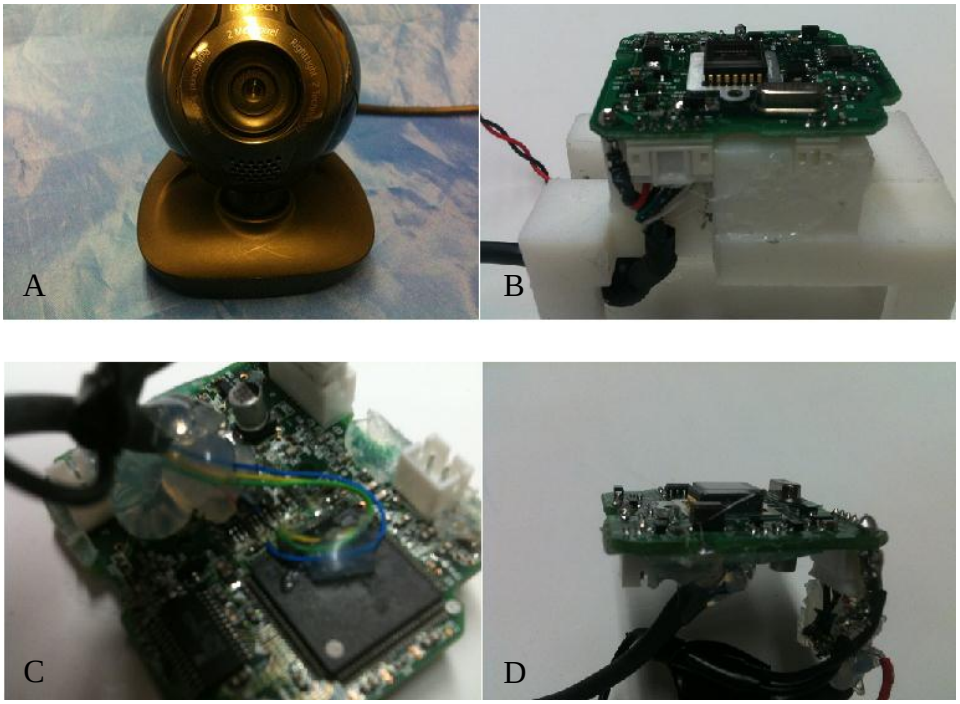


**Figure 12. Logitech webcam C 250 : (A) original , (B) lens-less detector, (C) modifications to circuitry to capture RAW data, (D) modified camera in test mount**

After some initial tests, it was concluded that this imager would be too noisy to detect the fluorophores at the concentrations that are required for clinical values of biomarkers such as CRP. A Fire I digital board camera with remote CCD (part # 2063) from Unibrain was then chosen for its ability to deliver the RAW data (Figure 13). The Fire I CCD is a ¼" CCD with square pixels and has a resolution of 0.3 Megapixels (1394a compliant, uncompressed VGA speed of 30 frames per second). This CCD also has a fully integrated electronic shutter with progressive scanning capabilities. One helpful feature of this CCD is its remotely located imaging head.

This allows the ADC and the post processing chip to be relocated and therefore does not become a design hurdle. The Fire I CCD also does not have a crystal on the array side of the detector, which, in some cases can interfere with the proper direct contact required for this type of detection method.

**Figure 13. Fire I CCD imager with remote head**

This CCD imager was integrated into a bench-top setup that was connected to a computer for image acquisition. In order to assure accurate results, the bench-top setup was automated with an Arduino microprocessor that was also connected to the computer in order to control the micropump and light sources required for the tests (Figure 14).

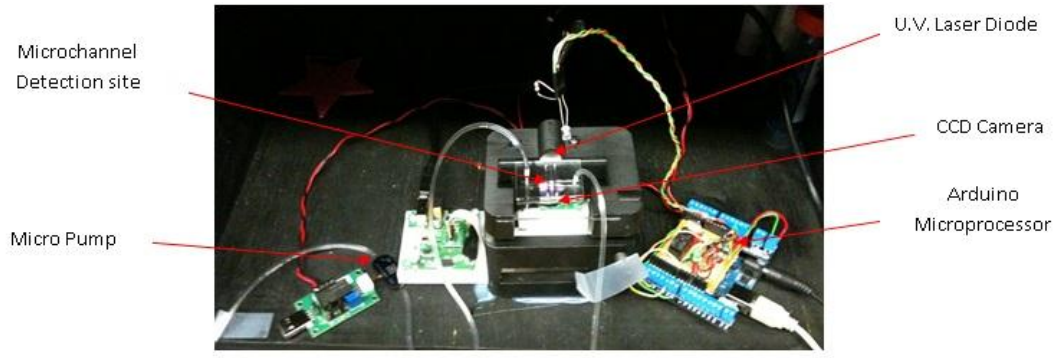


**Figure 14. Bench-top set-up with CCD holder, pump, controller and microprocessor**

A Matlab program was created to acquire the image from the CCD and to separate the data into individual color matrices. By separating the data and evaluating each color matrix, a quantitative analysis was performed to determine which colors are affected the most by the excitation of the fluorophores. A cutoff filter was placed between the detection site and the top of the CCD to block most of the excitation signals. Only by looking at the pixels, whose corresponding color coincides with the wavelength of light that the fluorophore emits, can a true representation of the detection site be obtained. An example would be that if we are looking for fluorescein, only the green pixels would be evaluated .The CCD imager captures the excitation light that is present in the detection site. Since most fluorophores emit light radially, there was no region of interests (ROI) defined and the size of the detection site was purposely made to fit within the boundaries of the CCD image.

The Arduino microprocessor was chosen because it can be controlled directly from Matlab. Since a Matlab program was capturing the images using one program instead of having multiple programs running at the same time, it was considered to be a much better option.

An Optical detector, just like any precision instrument, needs to be calibrated [43, 44]. This calibration or post processing was performed by capturing a RAW image, removing the dark frame image, and then dividing the resulting image by what is known as the Flat Field image.

$$\text{Calibration image} = \frac{(\text{RAW image} - \text{Dark Field image})}{\text{Flat Field Image}} \qquad (3)$$

The Dark Frame image is an image that is acquired with no integration time and the CCD is covered so no light can enter the detector. The Flat Field image is a dark image that is averaged over a time scale. The time scale that produced the lowest standard deviation in pixel values was 45 sec for this CCD detector. This calibration image was subtracted from all images that were acquired to provide consistent and accurate results. By calibrating the image in this way, most of the thermal and electrical noise was removed from each image.

When discussing system capabilities and characteristics an important variable is called the Limit of Detection (LOD). The LOD is defined as the concentration of analyte required to give a signal equal to the background pixel values plus three times the standard deviation of a black image pixel values [46].

$$LOD = (3 * STD) + Avereage \qquad (4)$$

The LOD was calculated by analyzing three chips that were filled with PBS Storage Buffer or isopropyl alcohol, depending on the solution in which the fluorophore was suspended. Three images for each chip were taken and the total summation of the pixel values was averaged. The standard deviation (STD) for each chip was calculated, and then the LOD for each detection system was determined. Calculating the LOD determines the minimum summation of pixel values that can be interpreted as a meaningful signal. Any summation of pixel values less than this LOD may have error associated with the instrumental measurement process would not be considered valid.

### 3.1.2 LOC Design for Optical Detection

The process that was used for the fabrication of the LOC is a process known as soft lithography. As mentioned in the introduction, the process of soft lithography is a simple and easy to perform process that involves creating a design in SolidWorks that represents the LOC. The file that is created is imported into a program called "Mastercam", which converts the file into machine language. The new program is run on a micro CNC milling machine. The milling machine mills the design into a piece of dimensionally stable polyvinylidene difluoride (PVDF)**.** Once the mold is fabricated, it is placed in a 20 percent solution of Sodium Hydroxide and water. The container with the solution and the mold is then placed in a sonicator for 6 hrs. to remove any residue and to remove any loose particles that could have been left behind by the milling process. Clear cellophane tape is placed around the perimeter of the mold to contain the PDMS. Thoroughly mixed PDMS is then poured into the mold with a 10:1 ratio of PDMS (Sylgard 184 from Dow Corning) polymer to curing agent [49]. The mold is then placed in a vacuum chamber at 27 inches of vacuum for 15 minutes to remove any bubbles that may have formed during the mixing process. The degased mold is then placed on a hot plate at 80 °C for 2 hours to complete the curing process. The cured PDMS is then peeled from the mold. All final modifications are performed such as punching the holes for the inlets and outlets. The upper and lower components of the chip are placed in a plasma asher for 5 minutes. The plasma asher process is one in

which the ionization of combustible products is removed from the surface of the PDMS to aid in the adhesion process. After the ashing process is complete, the two surfaces are aligned and pressed together. A final post bake for 2 hours at 80°C finishes the crosslink of the PDMS and completes the chip fabrication.

A modified PDMS microfluidic chip was developed to maximize the detection of the emission light emanating from the detection site. This involved creating channels or barriers, located around the waveguide and the detection chamber, that have a different index of refraction [50]. This technique allows most of the emission and excitation light to be well controlled (Figure 15). The new microfluidic chip includes an S-shaped channel to help alleviate the problem of bubbles which is one of the biggest issues that can occur on LOC devices [51]. The 250 x 200 micron S-shaped channel also increases the surface area of the detection site (Figure 15) allowing more capture anti-bodies to adhere to a functionalized chip.

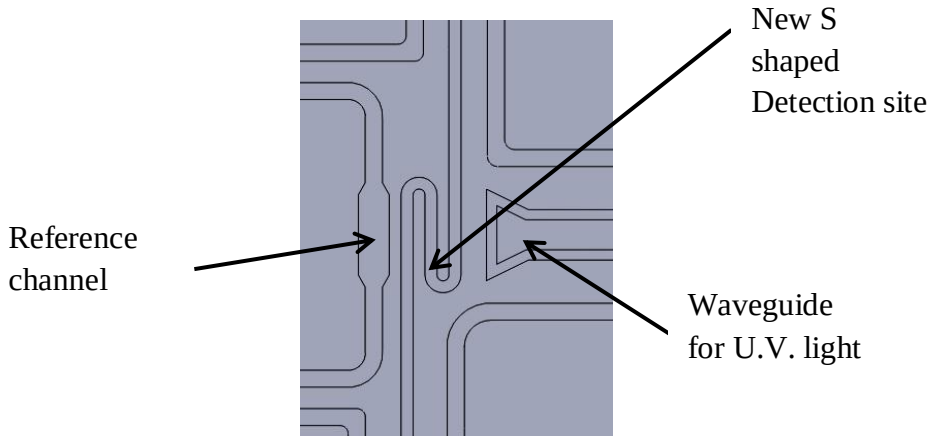


**Figure 15. Detection site with S-shaped channel and built in waveguide**

A major aspect of designing an LOC microfluidic chip is the integration of a waveguide to help channel the excitation light from the light source into the detection

site. The waveguide is created by surrounding a PDMS feature with an air gap [52]. The air gap contains the light that is passed through the PDMS, and transfer the excitation light to the detection chamber. The waveguide is equipped with a micro dispersion lens to help disperse the excitation light throughout the detection site.

During the experimental process, it was discovered that the interface between the waveguide and the light source was extremely critical. As a result, an optical waveguide aperture was implemented to channel the excitation light to only the waveguide. This technique was essential in reducing the auto fluorescing of the PDMS LOC by the light source and prevented excessive illumination [50, 51] .The waveguide aperture was crucially important when using the LED light sources, because most LED's have a 7 to 30 degree angle of dispersion. In **Error! Reference source not found.** the area in red indicates the detection site, the area in yellow indicates the waveguide, and the areas in blue represent the excitation light. It can be seen in Figure 16 A that without the waveguide aperture some of the excitation light is allowed to travel over the top and under the bottom of the waveguide. This extra light is then able to travel throughout the LOC. In addition, even though the blocking channels are placed around the waveguide, the waveguide aperture ensures that no light travels between the air gap and the blocking channels as seen in Figure 16 C. Figure 16 image B (Side View) and D (Top View) represent optimal focusing of excitation light for the most precise results.

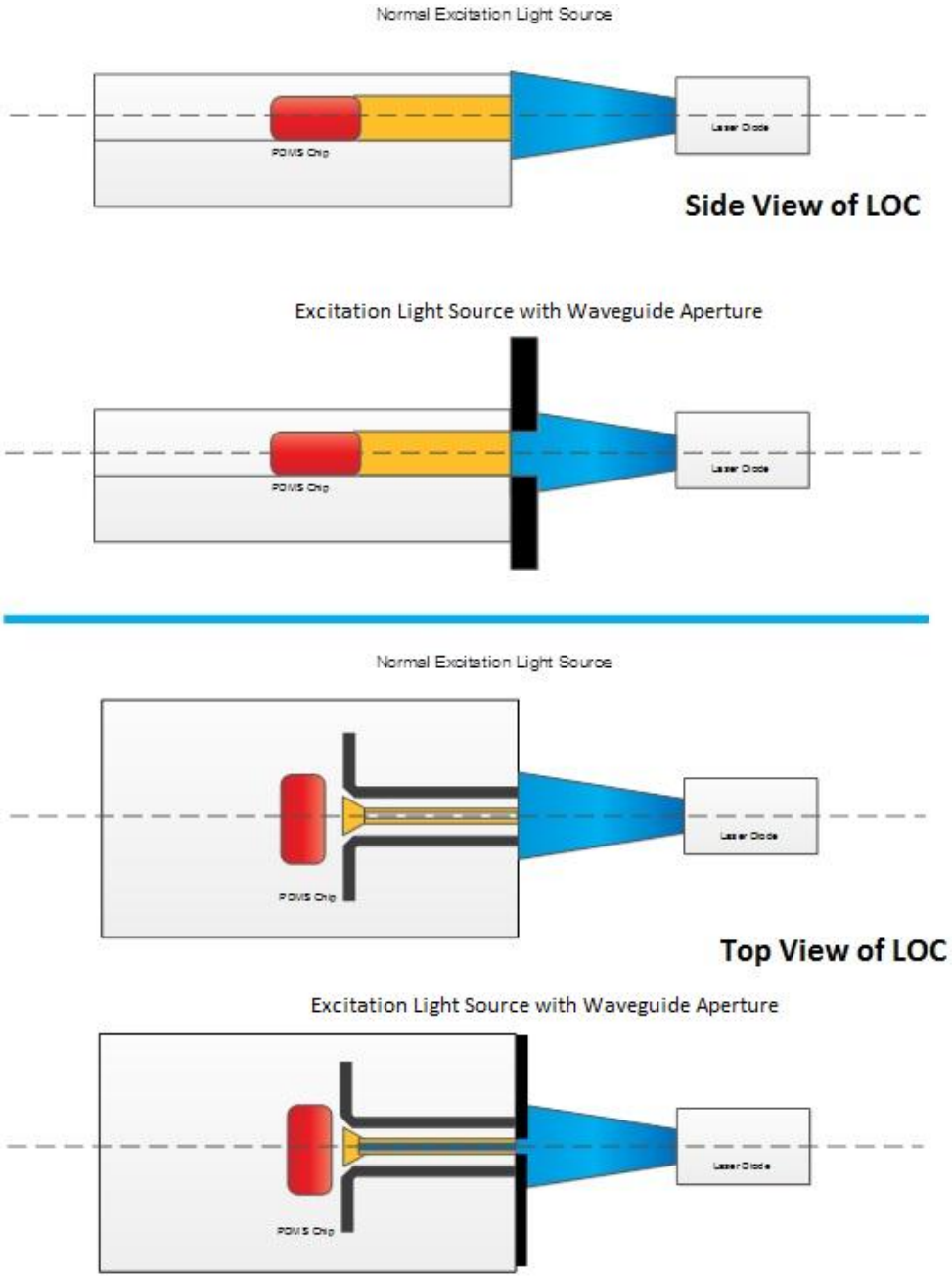


**Figure 16. Interface of excitation light source and LOC waveguide. A and B are Side views and C and D are Top Views of the microfluidic chip showing the center line of the excitation light source**

### 3.2 Fluid Handling

One significant advantage of using a CCD imaging device is that it can be used to control the timing of the biological reagents as they pass through the detection chamber. It is extremely important to control the fluids necessary to complete an accurate on-chip immunoassay. The significance of this cannot be understated as this system uses an active pumping scheme. A POC device with its onboard CCD camera is capable of providing instantaneous fluid control using a custom feedback loop. A custom program created in Matlab controls the Bartels micro pump and a series of off chip micro-relief valves. Previous POC systems that have been evaluated used timing algorithms to move the sample and reagents around the chip but that proved to be extremely unreliable and inaccurate.

The Pumping scheme used is a closed loop system with 2 three-way micro valves to control which sections of the chip are used. Figure 17 shows an illustration of the closed-loop pumping system with the Bartels micropump. When micro-valve B is switched and it closes tubing 3, the pump will pull a vacuum on the bottom of the chip. This will begin the pumping process and start to pressurize the output. At the first step, valve A is closed and the sample is allowed to flow through the chip. Once the sample has passed through the detection site, valve A is switched, and it opens tubing 1 and closes tubing 2. Once tubing 1 is open the biological reagents start to pass through the LOC.

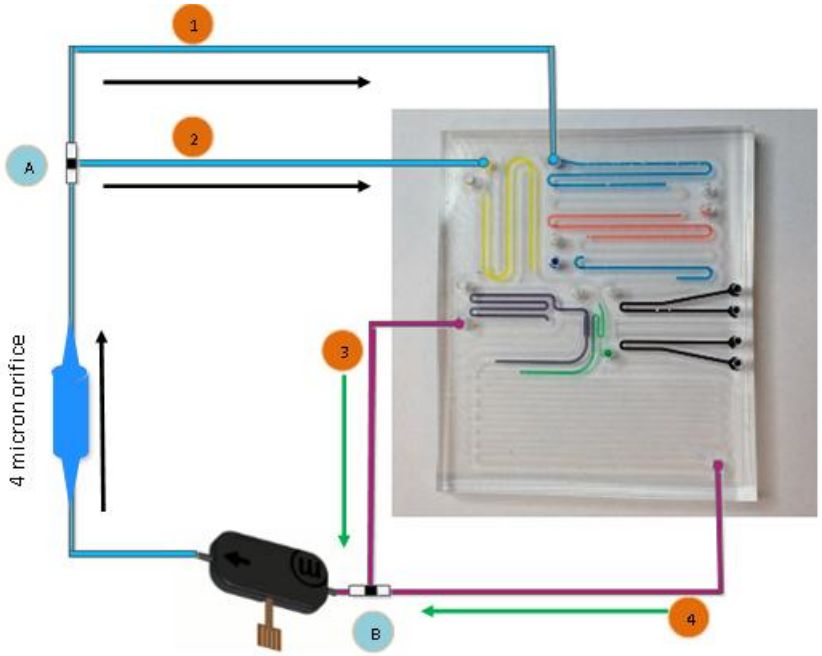


**Figure 17. Pumping schematic of LOC with micropump and inline 4 micron orifice**

A micro orifice with a 4 micron diameter was installed in line with the micro pump. This orifice reduces the flow rate to allow the CCD imager enough time to determine which reagent is in the detection site.

The fluid handling scheme that was employed uses an LED directly above the detection site to illuminate the detection chamber. This feedback control system is able to detect the presence of fluid in the detection chamber and is able to move the biological reagent through the microfluidic chip with great accuracy by turning the pump on and off. The on-board CCD device also allows a POC device to ensure that it

is evaluating the appropriate detection area eliminating any errors that might have occurred in the manufacturing of the LOC's

The optical detection of clear liquids is somewhat difficult as it is not easy to distinguish a clear liquid against PDMS, because both are translucent. During some experiments with the optical detection aspect of the project, it was noted that when there was a clear liquid in the detection zone there was less extraneous "noise". In Figure 18 on the right side of the image, a histogram of the detection site pixel values can be seen. Figure 18 A shows the detection site with air in the main channel as well as in the reference channel. The image of Figure 18 B shows liquid in all the channels, and Figure 18 C show air in the reference channel and air in the main channel. When there is the presence of a clear liquid in the channel, it is difficult to distinguish the walls of the channel and the liquid itself as seen in Figure 18 B. Figure 18 A shows a definite distinction between the walls of the channel and the air. The pixel values when there was air in the channel had some "noise", the pixel values were not consistent, and they had higher values when compared to pixel values when there was the presence of a clear liquid. The control system that was designed took advantage of this increase in noise by comparing the signal from the detection site with the initial signal containing a clear storage buffer solution. (The clear storage buffer was used to prevent the detection site from drying out between the time of the manufacturing process and the time when the LOC was used.)

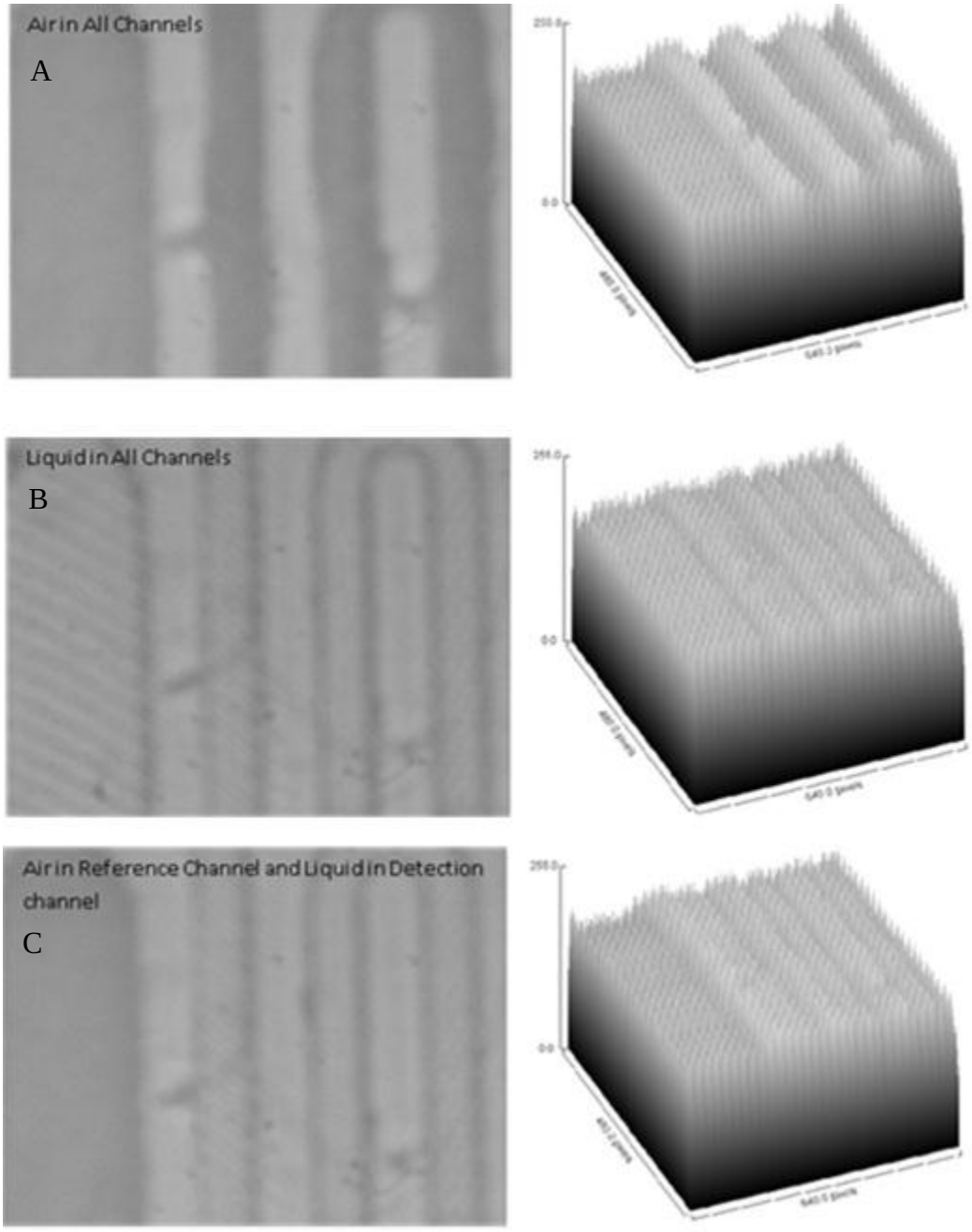


**Figure 18. Image of Detection chamber using white diffuse light for liquid detection**

The first step in controlling the fluid on a microfluidic chip is to identify the microfluidic channels and determine a Regions of Interest (ROI). This ROI is located

just inside the walls of the microfluidic channels. This step eliminates any false signals due to the fluid - PDMS interface. The microcontroller turns on an LED and an image is acquired with the presence of a storage buffer in the detection chamber. This technique provides a baseline image for comparison. Newly acquired images are constantly being compared to the baseline image and the difference between the pixel values is converted into a binary matrix. To convert this into a binary matrix, a threshold value is determined. For any values less than this threshold the values are converted to zeros. For any values higher than this threshold, the values are converted to ones. To determine if a liquid is present, a comparison of the total number of zeros to the total number of ones is made. A value of zero indicates that there is no change between the new image and the baseline image. If there were more ones than zeros, this indicated the presence of air. Knowing the sequence of the fluids and air gaps to be used, a proper sequence of commands can then be made to activate the micro pump and micro valves.

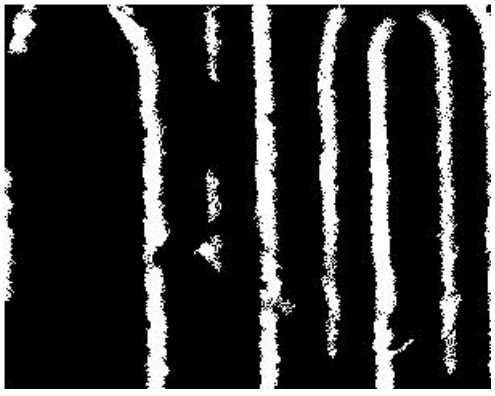

**Figure 19. Binary image of detection site; the black indicates the S - shaped channel and refrence channel while the white indicates the walls of the microfluidic chip**

Figure 20 represents the flow chart command structure for the pumping feedback control system. Once the program is initiated, several control images are acquired to be used for the Dark Field images, the Dark Current images and the control image. Once the images are acquired, the Matlab program analyzes the images and finds the important ROI. The next command determines if the program is running in the reference channel or the actual test. Depending on the condition, the program selects the reference channel program or the S-shaped detection program to initiate. The program acquires another image to determine the type of substance in the detection site (air of liquid) by comparing it to the control image. The program now goes into a loop situation of acquiring images, comparing each image to the control image while constantly looking for presence of air. Once air is found, the program is flagged or changes the state (control flag) to liquid. The program again goes into a loop situation and now is looking for air while acquiring images and comparing them to the control image. Once a difference is detected between the images, the state is changed to liquid and the pump is turned off. If at this point the program has only run through the program commands once and is not in the final stage, the program will begin the loop program again and start looking for air again and keep running the loop. If the program is in the final stage, it starts the detection loop for the analysis of the immunoassay. If the program is still in the reference channel loop, the program will loop back around to the beginning and run again until it completes all the immunoassay steps. If the program is not in the reference loop it will start the analysis of the results and send the results to the custom Python program for distribution of the results to the smartphone, e-mail, or text.

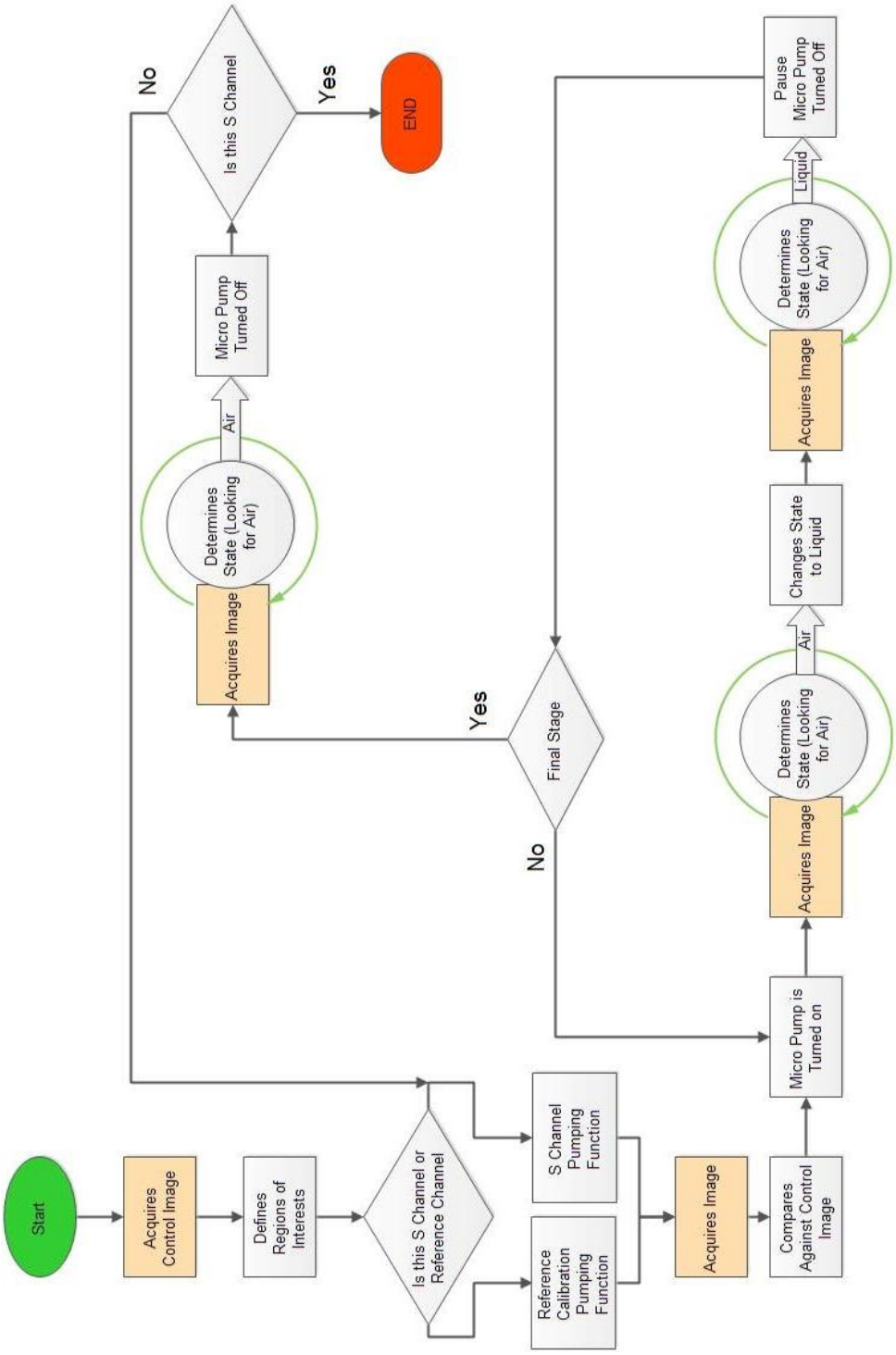


**Figure 20. Flow chart of matlab commands for active pumping system**

### 3.3 Wireless and iPhone Integration

The way that communications enter the World Wide Web is through internet portals. For wireless communication, the portals are in the form of a router. To foster simplicity and good communication speed, a wireless network was created using a Linksys WRT54GL Wireless-G open source Router. This router network was the link to all the different devices such as the HBLD, the iPhone and the computer

The creation of an iPhone app was done using the Apple iOS SDK program available through the Apple iOS Dev Center. This SDK program allows the user access to a complete development environment which includes the base X code, iOS simulator and interface builder. A program called X code is the basic user interface, and it is programed using the objective C computer language. The iPhone App that was developed allows the user to control the HBLD POC device, input user information, get status updates and display results. Figure 21 shows an illustration of the wireless protocol. Step 1 inputs the user information and selects the desired test. Once completed, a signal is sent out to the HBLD to activate the test (Step2) and to initiate the Matlab program. There is constant back and forth communication between the HBLD (Step2) and the Matlab program (Step 3). Once the test has been completed the Matlab program will send the results to a Python program which will deliver the results to the smartphone or predetermined computer file (Step 4).

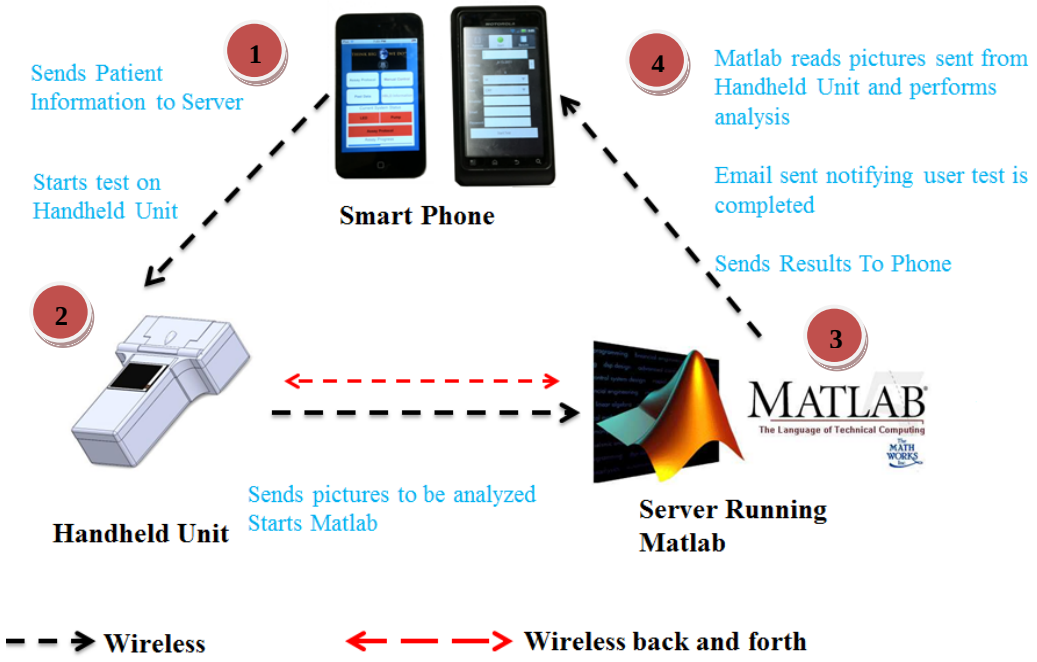


**Figure 21. Illustration of command protocols for HBLD system**

A computer algorithm Start_matlab_server.py was created using a program called Python to control the interface between Matlab and the web server. This program, when initiated, listens for a signal via the web server from either the HBLD or the iPhone App. Once the signal is received, the custom Python program opens Matlab and runs a custom computer algorithm called HBLD.m. This HBLD program contains all the necessary commands to run a complete LOC immunoassay in the hand-held HBLD. The hand-held POC device has a program built into it that communicates back and forth to Matlab via the wireless network router. Figure 22 shows the command structure that the Python program follows.

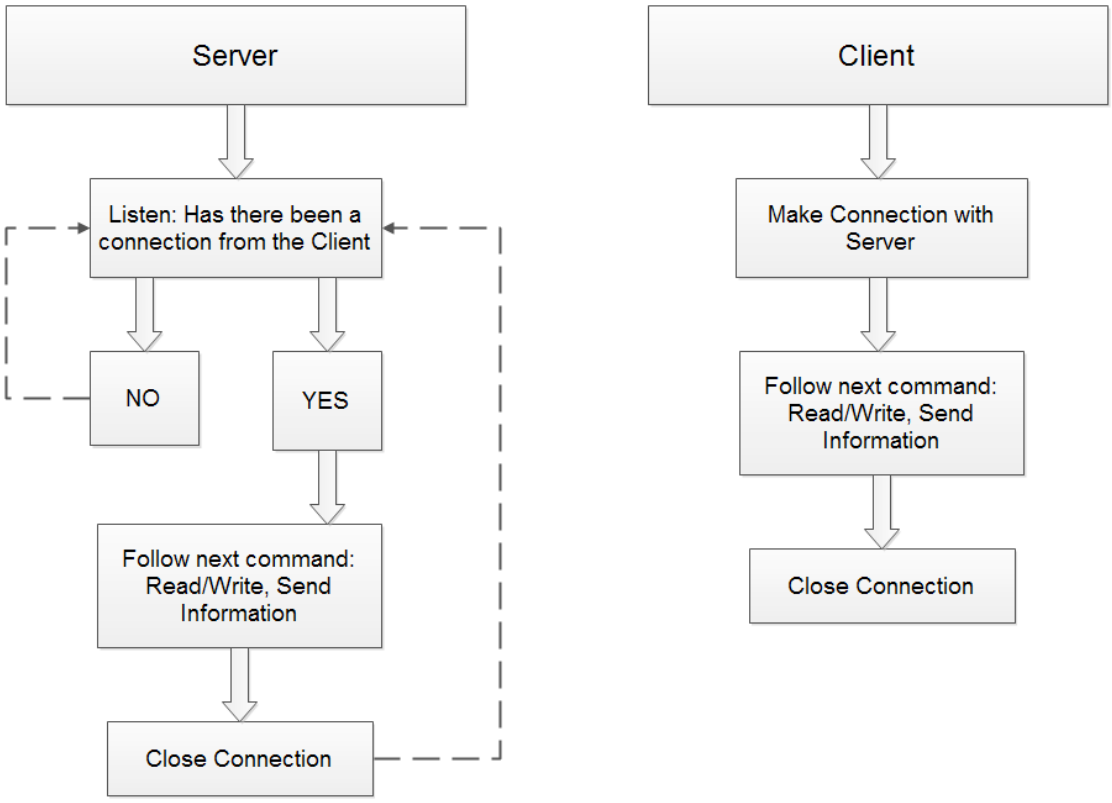


**Figure 22. Command protocols for Server/Client**

### 3.4 Assay Protocol

Part of the HBLD detection system involves the development of an assay that will perform the standard fluorescence immunoassay test which would ordinarily be performed in a biological laboratory. The immunoassay is that of the heterogeneous, sandwich type. A multilayered functionalization is built up on the surface of the microchannel and includes the following layers: Bovine Serum Albumin (BSA), Glutaraldehyde and Protein A. This offers a surface with a high affinity for the region of the capture antibody in the heterogeneous immunofluorescence assay. The functionalization of the chip starts with a clean PDMS microfluidic chip. While the actual test takes minutes, the preparation of each functionalized chip takes quite a bit longer. The chips can be prepared ahead of time as explained later on. The following steps are performed at room temperature: Step1. 1.5 mg/ml of BSA is added to 1x PBS, and then injected into the detection site and allowed to incubate for 4 hrs. Step2. The detection site is flushed with PBS and then air aspirated to remove any unbound material. Step3. A 0.4 volume to volume solution of Glutaraldehyde to water is injected into the detection site and allowed to incubate for 1 hr. Step4. The microfluidic chip is rinsed and aspirated before a solution of 100 µg/ml of protein A and 1x PBS is injected into the detection site. Step5.The solution of Protein A is allowed to incubate in the detection site for 1 hr. Step6. The chip is again rinsed and aspirated before the final storage buffer is injected into the detection site. Step7. The chip is then sealed with clear tape to prevent any evaporation of the storage buffer. Step8. The chip is then stored in a refrigerator at 34 degrees F and is now ready for use as a functionalized LOC.

The assay protocol for the detection of CRP starts by introducing the capture antibodies into the pre-functionalized detection site. The capture antibodies link to the altered surface, oriented with the variable region towards the channel to offer optimal binding to the antigen, CRP. The CRP from the sample binds to the capture antibody, which is an anti-CRP, polyclonal antibody raised in rabbit. Next a biotinylated anti-goat CRP polyclonal antibody binds to the immobilized CRP on the surface of the microchannel. Qdots were selected as the fluorophore for this CRP test and the Qdots were conjugated with Streptavidin. The Qdot binds to the built-up chain on the surface through the biotin/streptavidin affinity, which is an extremely strong and reliable bond (Figure 23). The concentration of CRP in the sample is ascertained through a standard curve based on a correlation between CRP concentration and the signal received from the Qdots using the CCD to measure the signal. The capture antibodies are rabbit anti-human CRP (ab31156) from Abcam Inc. The detection antibodies are Biotinylated goat anti-human CRP (CRP30B-G1b) from Academy Biomedical Company. The CRP (30R-AC067) are from Fitzgerald Industries International. The Streptavidin coated Qdots 605 ITK (Q21701MP) are from Invitrogen Corp. The reason that the rabbit anti-human and the goat anti-human were selected was because these two antibodies do not have a high affinity for one another.

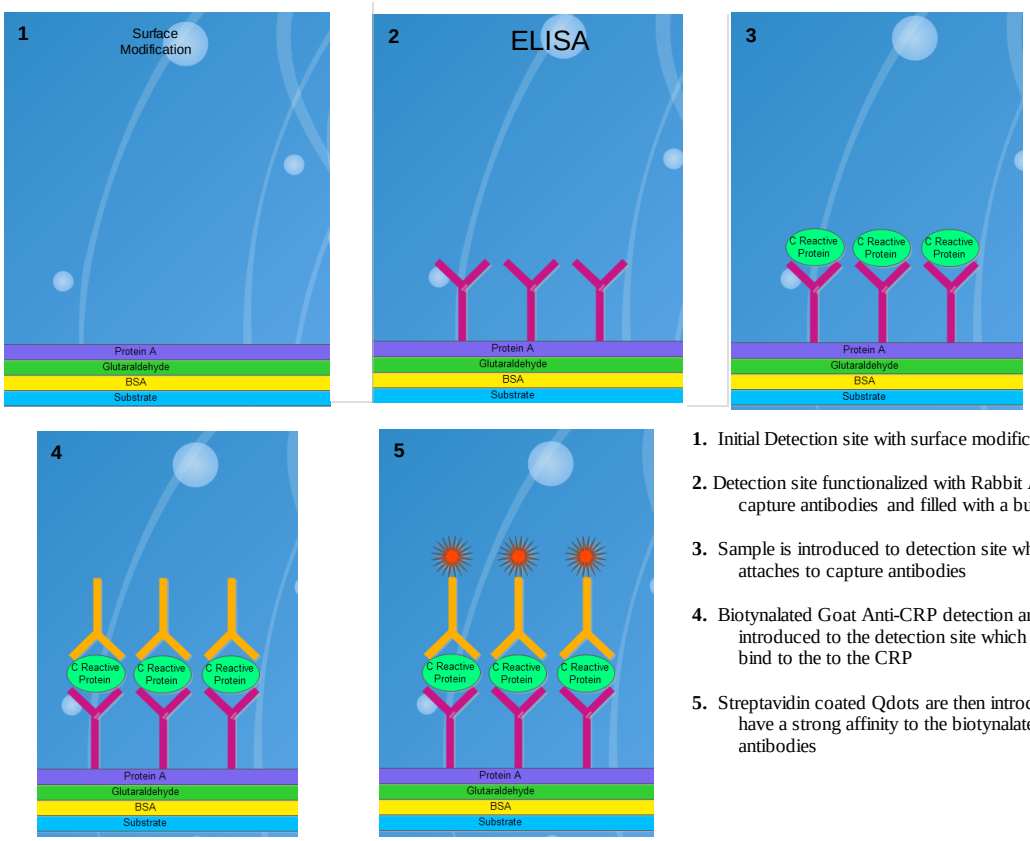


1. Initial Detection site with surface modifications
2. Detection site functionalized with Rabbit Anti- CRP capture antibodies and filled with a buffer solution
3. Sample is introduced to detection site where CRP attaches to capture antibodies
4. Biotynalated Goat Anti-CRP detection antibodies are introduced to the detection site which will bind to the to the CRP
5. Streptavidin coated Qdots are then introduced which have a strong affinity to the biotynalated detection antibodies

**Figure 23. Sandwich assay protocol for detection of C-reactive protein in buffer solution**

### 3.5 Hand-held POC device

A prototype detection device that uses the lens-less CCD detection method described earlier was constructed to show the viability of this method of detection. The device was built around a hand-held platform that provided reliable and repeatable results. The HBLD device is a wireless, self-contained, portable, and easy to use device. To use the device one needs simply to insert the microfluidic chip loaded with a sample and initiate the test from a smartphone device that is loaded with appropriate iPhone App. The HBLD will run a preloaded program that is stored on the onboard microprocessor of the HBLD and will initiate contact with a server which is running Matlab. The server will begin to run a series of tests while it is continuously updating the HBLD with new commands. The results will then be delivered to the iPhone App and to an appropriate secured email account.

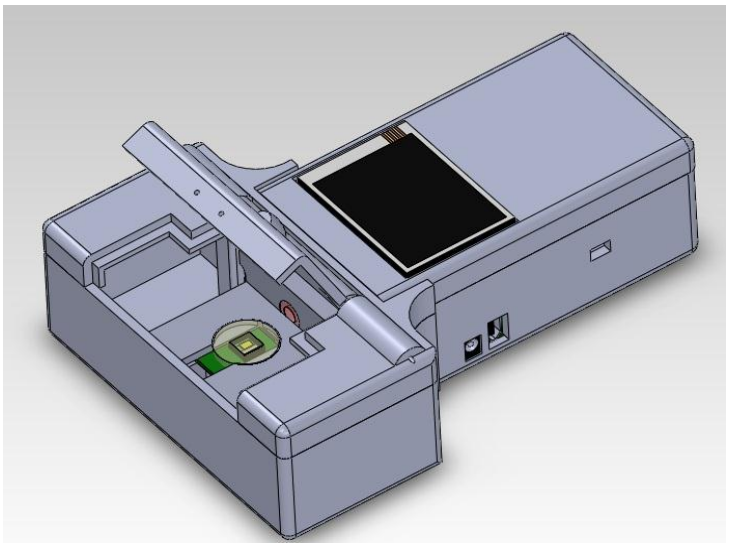

**Figure 24. Hand-held lens-less biological detector HBLD**

The HBLD prototype device is constructed from a variety of components. A cutaway view of the device with its hardware components can be seen in Figure 25.

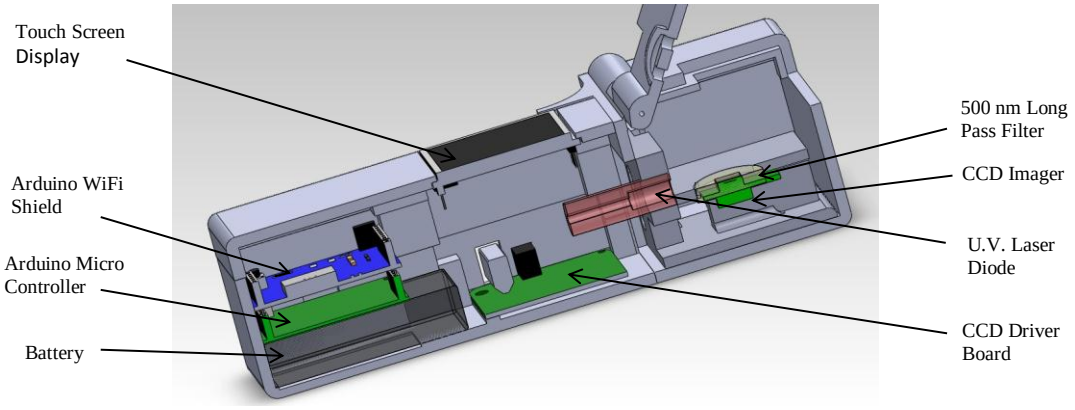


**Figure 25. Section view of HBLD showing placement of hardware components**

The HBLD device has an onboard microcontroller known as an Arduino Mega 2560. Arduino is an open-source single-board microprocessor with an Atmel AVR processor designed to make the process of using electronics more accessible. The Mega (Figure 26) is a microcontroller based on the popular Arduino Duemilanove but with an increase in inputs and outputs as well as multiple hardware serial ports. The Mega has 54 digital inputs/outputs of which 14 can be Pulse Width Modulated (PWM). The Mega has 16 analog inputs and a 16MHz crystal oscillator. The Mega also has 256 KB of flash memory and 4 KB of onboard memory called EEPROM. The Mega operates on an external power supply of between 6 and 20V DC. The Arduino Nano Mega has the same features as the Mega 2560 but with a reduced overall size of 30 percent. The dimensions of the Nano Mega are 71mm x 53mm x 11.3mm. The main advantage of the Mega over the Arduino Duemilanove is that it has four hardware serial ports (Universal asynchronous receiver/transmitter, UART's). The

multiple UART's allow the user to communicate simultaneously with multiple devices. This will be crucial when using a touchscreen and Wi-Fi shield. The digital outputs have the ability to deliver up to 40 mA of DC power at 5V.

The Arduino hardware is programmed using software similar to C++ in syntax and use of extensive libraries. The software has a built-in standard programming


**Figure 26. Arduino Mega microprocessor**

language compiler, which is able to communicate with a boot loader that is preprogrammed on the Arduino. The Arduino programming language has the ability to communicate with other programs such as Matlab.

The Arduino family of microcontrollers has many available add-ons called "shields". One important shield is the wireless communication shield called "The Copperhead" (Figure 27). The Copperhead Wi-Fi Module is 802.11b certified and can support transfer data speeds of 1 and 2 Megabyte per second (Mbps). The Wi-Fi module supports both infrastructure and ad hoc wireless networks with both 64-bit and 128 bit Wired Equivalent Privacy (WEP) security algorithms. The Wi-Fi module communicates via SPI (pin interface) with onboard slave select (SS), system clock line (SCL), clock speed (CLK), master in slave out (MISO), and master out slave in (MOSI) pins allow for easy configuration with the Arduino boards and UARTs. The

ability of the Wi-Fi module to interface in server-client mode allows the module to be easily set-up using the Wi-Fi libraries and is relatively inexpensive at around $56.

The Mega microcontroller that was selected needed to be modified to be able to communicate with the Copperhead Wi-Fi shield. This was accomplished by

**Figure 27. Copperhead Wi-Fi Shield**

rewiring the previously mentioned SPI pins. The following alterations relocated the connections between the Mega and the Wi-Fi shield: SPI pin 50 (MISO) needed to be connected to pin 12 on the Wi-Fi shield, pin 51 (MOSI) needed to be connected to pin 11, pin 52 (SCK) needed to be connected to pin 13, pin 53 (SS) needed to be connected to pin 10 and finally pin 21(SCL) needed to be connected to the Wi-Fi shield pin 2. The modification can be seen in Figure 28.


**Figure 28. Modifications to Arduino Mega and Copperhead Wi-Fi Shield**

Another Arduino add-on shield that was used in the construction of the HBLD is the Liquidware's Touchscreen slide (Figure 29) graphic user interface (GUI). The Touchscreen slide GUI has a bright OLED screen with a touchscreen pad on top of the display. The Slide has its own microprocessor on board to act as a graphics processor. The Touchscreen slide features a 320 x 240 OLED display with resistive touch capabilities for precise viewing and tactile sensing. The shield is UART compatible and easily programmed with the downloadable graphics library.

**Figure 29. TouchShield Slide**

An ultra violet laser diode with a 405 nM wavelength is used as the excitation light source for the on chip fluorescence detection. The HBLD uses a 405 nM Blu-ray U.V. laser diode with 100 mW of output power. The PHR-908T laser diode produced by Sanyo Electric Co. Ltd. has a stable linear output compared to the input current of up to 100m A.

PHR – 805t

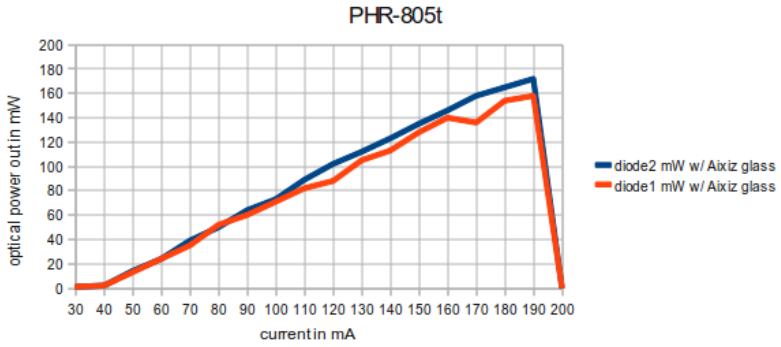


**Figure 30. Sanyo 405 nM laser diode and output specifications**

The laser diode is contained in an Axis laser module. This module provides a stable platform for mounting in the HBLD and will play a vital role in dissipating the excessive thermal energy that the laser diode emits. One inherent problem with laser diodes is that they require a stable input current. A Groove 2 (25-500mA) linear driver board with adjustable output is used to drive the U.V. laser diode and allows for final, fine tuning to achieve the best results.

# CHAPTER 4

# FINDINGS

## 4.1 Optical Detection

This section of the research project involves the detection of various fluorophores including FITC, Phosphor Dots and Qdots. Several different CCD imagers were analyzed for each of the fluorophores and the LOD for each one was calculated. The type of fluorophore and the type of CCD were changed to determine which combination was able to be used for the detection of CRP. Each detector required a different excitation light source and a different optical filter.

The first set of experiments that was run was for the detection of FITC using the bench top set-up, as shown in chapter 3, with the Logitech C210 webcam having the lens removed. The bench top set-up used a 500 nm blocking filter (Edmunds Optics # 47616). For the excitation light source a 495 nm, 3 watt LED (CREE # C503B-BAN-CY0C0461) was used. For this test FITC had an emission wavelength of 521 nm and only the green pixel values were evaluated. The LOD for this detection setup was 52μM with this value being higher than the normal clinical value assuming a one to one binding ratio of CRP to FITC. The results can be seen in Figure 31. These results were similar to results that a colleague, Kelly Cook, achieved with her lens-less CCD detector for the detection of FITC.

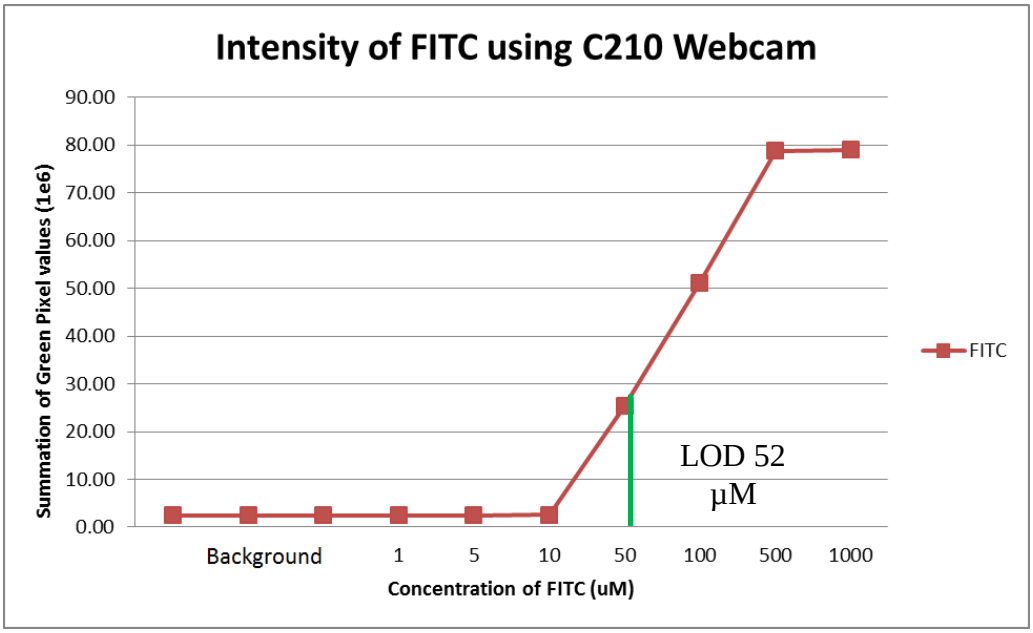


**Figure 31. Detection of FITC with a Logitech C210 webcam**

Next, the modified webcam was used for the detection of FITC in PBS buffer. As before, the background noise level was observed and recorded. However, the modifications to the webcam generated a large amount of extraneous noise. Both the unmodified and the modified webcams had the lens covered for the evaluation of the noise for each pixel value. A comparison of the unmodified webcam to the modified webcam was observed and can be seen in Figure 32. The figure shows that the unmodified webcam had some noise up to a pixel value of 17, while the modified webcam had noise up to a pixel value of 24. Since the total scale of the pixels is 0 to 255, the noise in the modified webcam corresponds to approximately10 % of the total signal values. For most imaging, an acceptable noise level is around 2-3 %. With the noise being so high the modified webcam was not used for the detection of FITC.

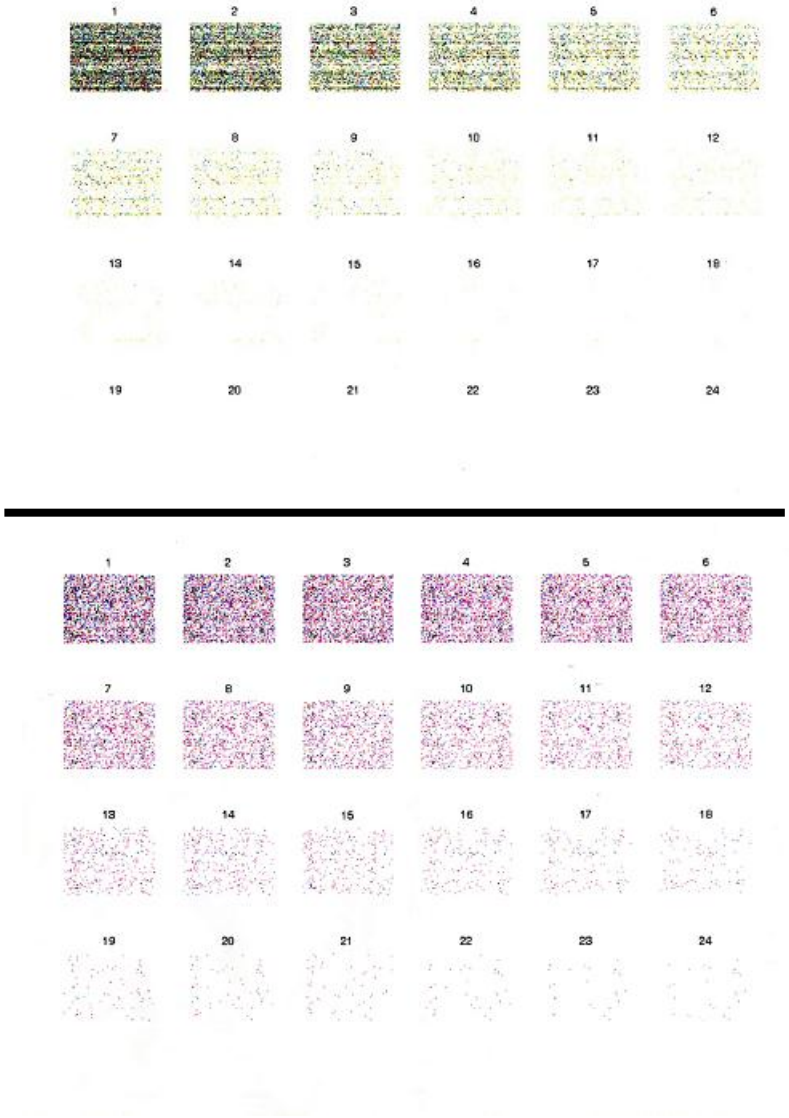

**Figure 32. Pixel noise from unmodified (top) and modified (bottom) webcam with lens covered**

A set of experiments were performed for the detection of FITC with the Fire I CCD imager. The same excitation light source and the same optical filter were used as in the previous experiments.

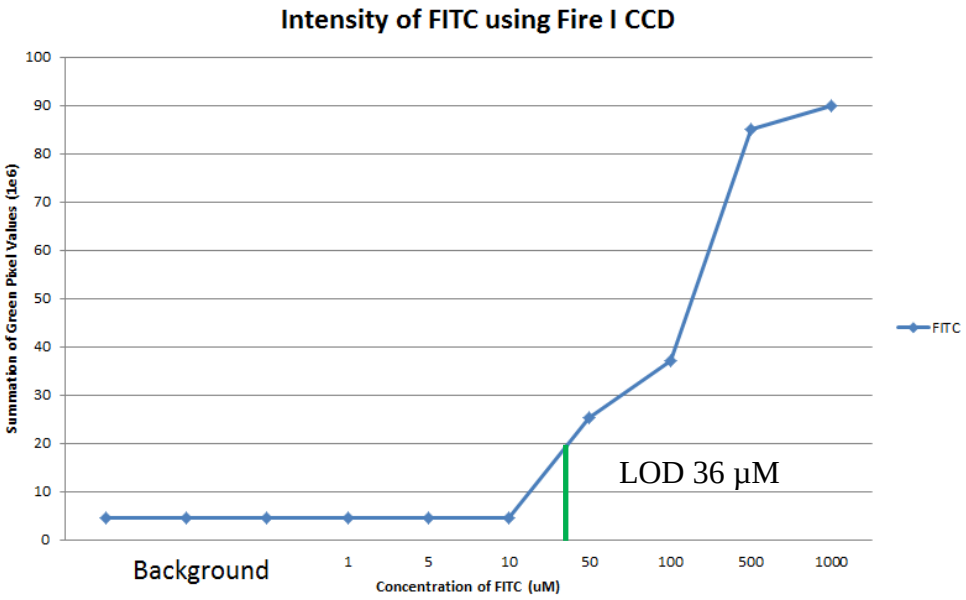


**Figure 33. Detection of FITC with a Fire I CCD imager**

The next set of tests was run was for the detection of Europium Doped Yttrium Vanadate Phosphor dots. The same bench-top setup was used substituting a 607 nm cutoff filter (Edmunds Optics # 84102) in place of the 500 nm filter in the previous test. A U.V. LED (Fox # FG350-R5.5-WC015) was used as the excitation light source. Phosphor dots employ a 350 nm excitation light source and have an emission wavelength of 617 nm. Only the red pixel values of the lens-less CCD were analyzed. Concentration levels of phosphor dots in PBS were loaded into the detection site. The summation of the red pixel was recorded. Figure 34 shows the results of the different

concentration levels vs. the summation of red pixel values. The Phosphor dots have a molecular weight of 203.84 mg/ml. The LOD for Phosphor dots was determined to 6.38µM.

A desktop spectrometer from Ocean Optics, model USB 4000, was also used for the detection of Phosphor dots to compare against the CCD detector. The results are shown in Figure 35. A third order polynomial curve fit equation was found for both graphs. The resulting curve fit equations were used inserting the original values into these and plotting the results. The y axis of the graph was also changed to a logarithmic scale in order to evaluate the results shown in Figure 36. The figure shows that even though the magnitude of the scales of each of the detectors is different the overall shape is the same.

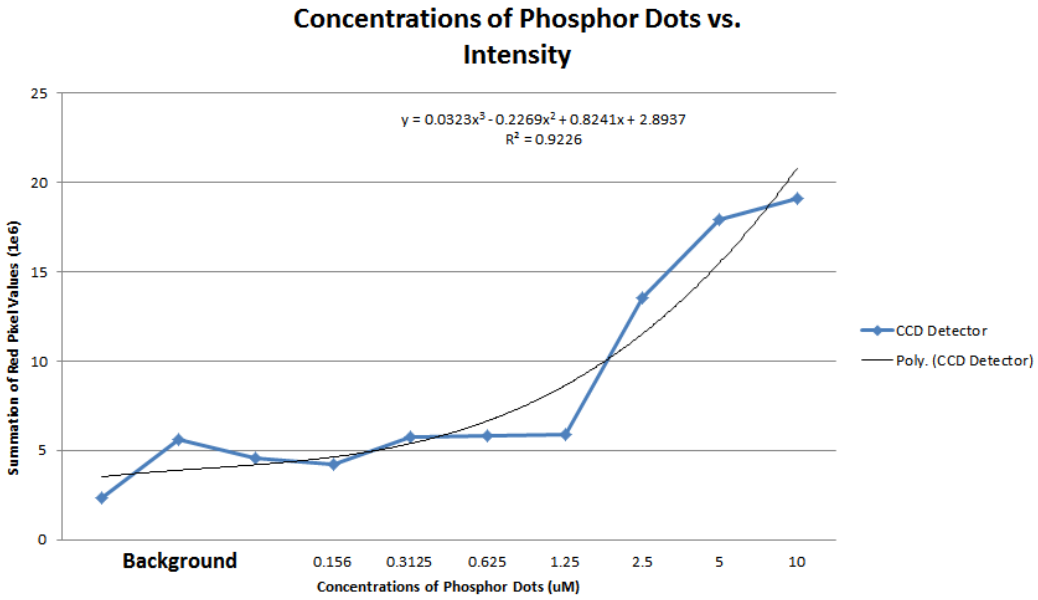


**Figure 34. Concentrations of Phosphor Dots vs. Intensity using lens-less CCD**

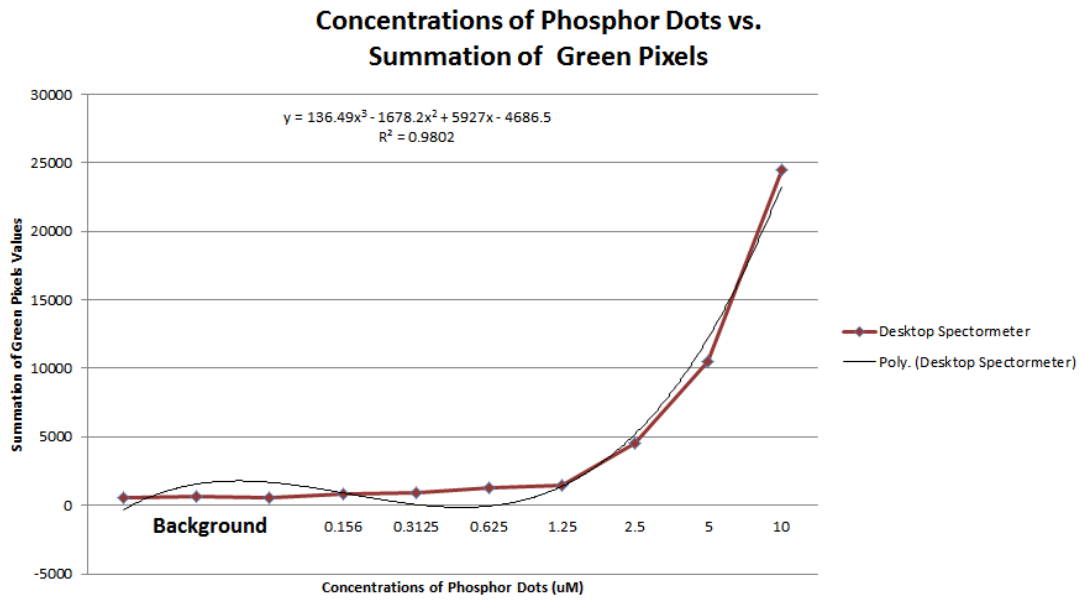


**Figure 35. Concentrations of Phosphor Dots vs. Intensity using Desktop Spectrometer**

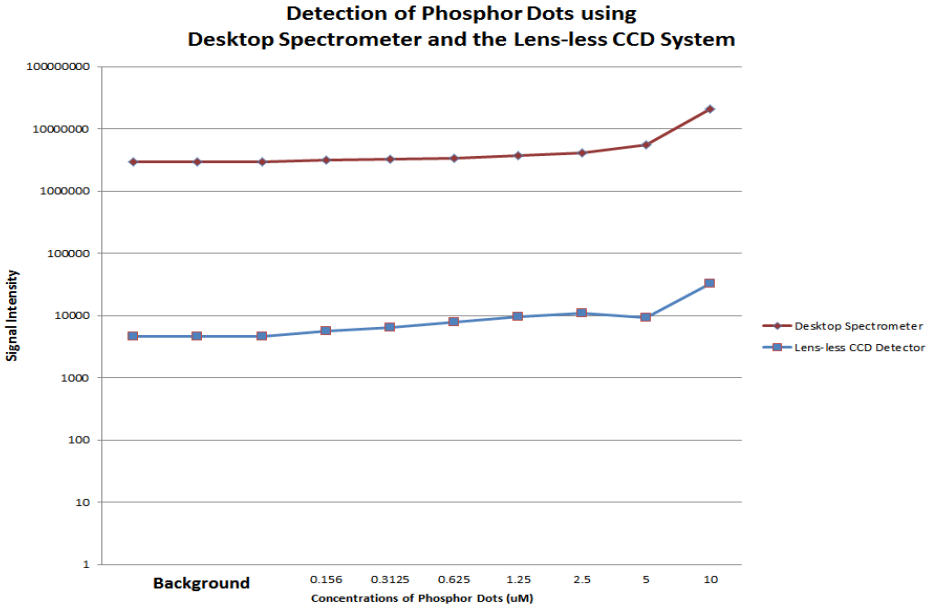


**Figure 36. Comparison Desktop spectromer and lens-less CCD for the detection of Phosphor Dots**

The next fluorophore to be evaluated was one of Qdots in alcohol. The bench top set-up was used with a 607 cutoff filter from Edmunds Optics. The Qdots were suspended in isopropyl alcohol and thoroughly mixed. Some initial tests were performed to verify that the lens-less CCD was able to detect Qdots at concentration levels between 0.001µM and 0.5 µM. Figure 37 shows that the lens-less CCD was able to detect Qdots near a level as low as 0.001 µM.

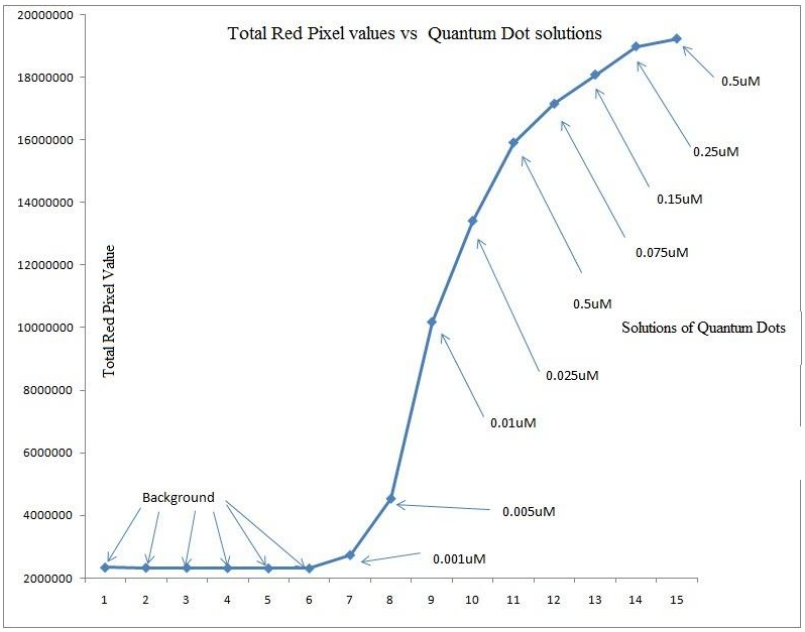


**Figure 37. Concentrations of Qdots in Alcohol vs. Intensity**

Figure 38 and Figure 39 show the actual image that the Fire I CCD acquired in the detection of Qdots at several different concentrations .The detection of Qdots in alcohol at different concentrations was performed on the bench top apparatus and the concentrations vs. the summation of red pixels can be seen in Figure 40. The figure shows that he LOD for Qdots in alcohol, with no waveguide aperture, was 1.901 nM.

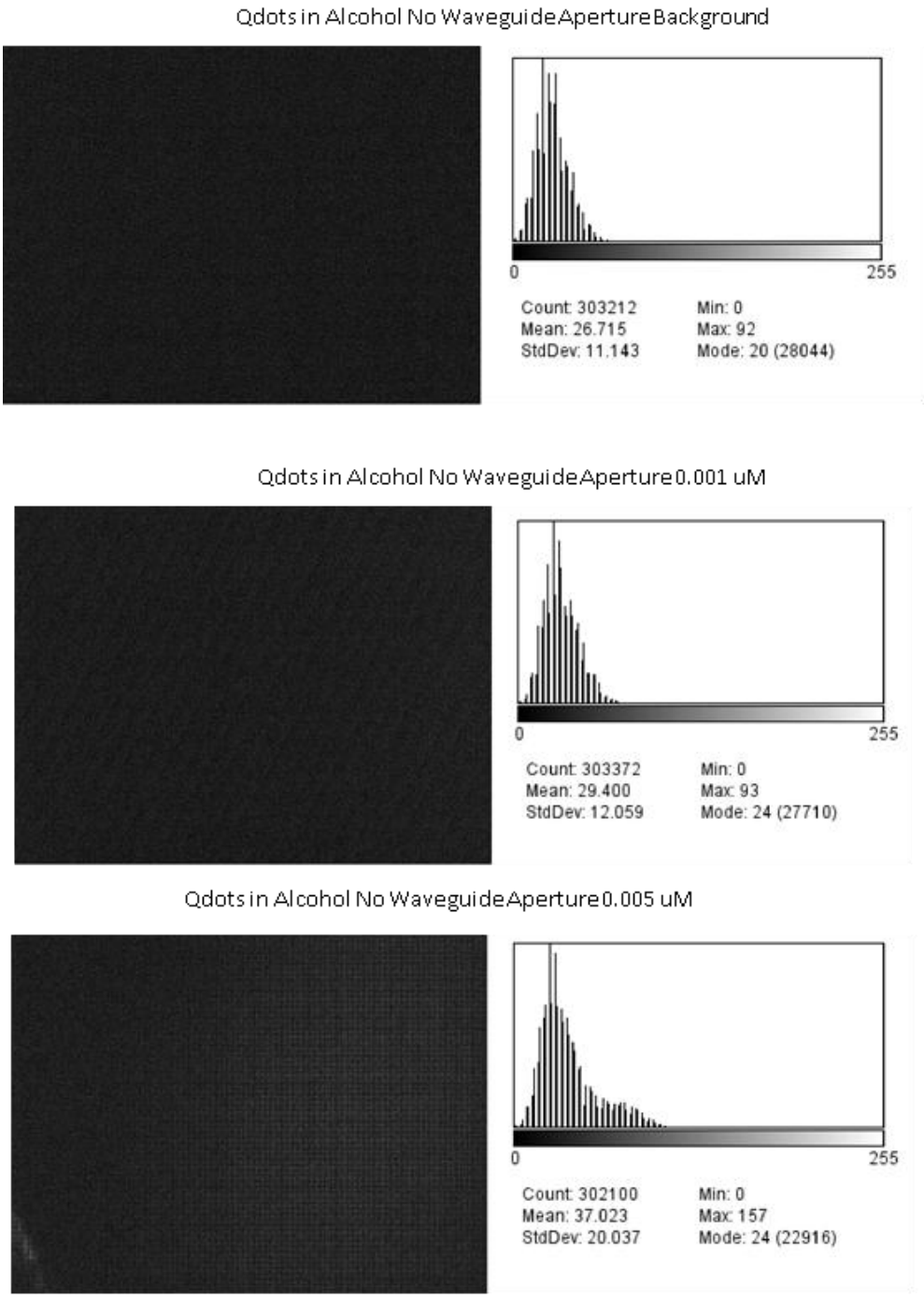


**Figure 38. Actual CCD image for different concetrations of Qdots in alcohol along with histogram of pixel values (no Aperture)**

Qdots in Alcohol No Waveguide Aperture 0.01 uM

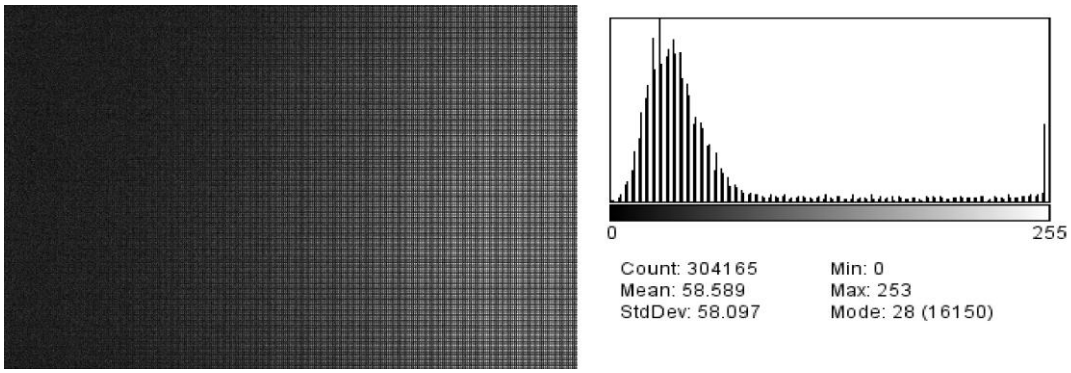


Qdots in Alcohol No Waveguide Aperture 0.05 uM

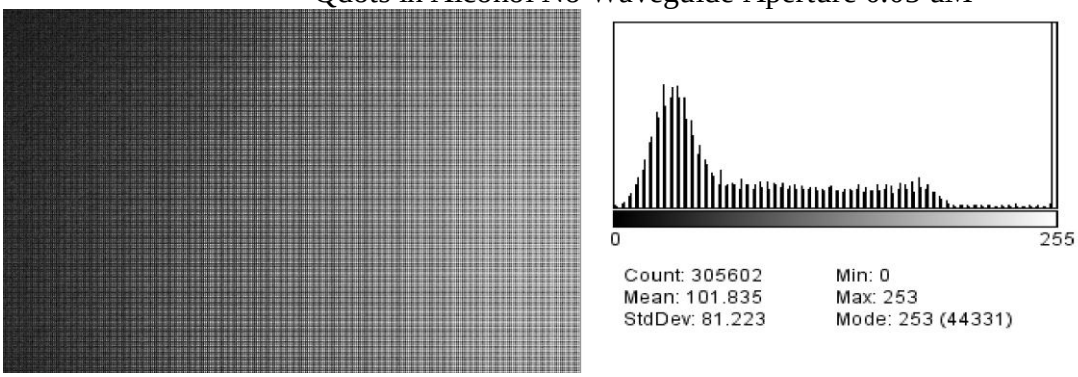


Qdots in Alcohol No Waveguide Aperture 0.1 uM

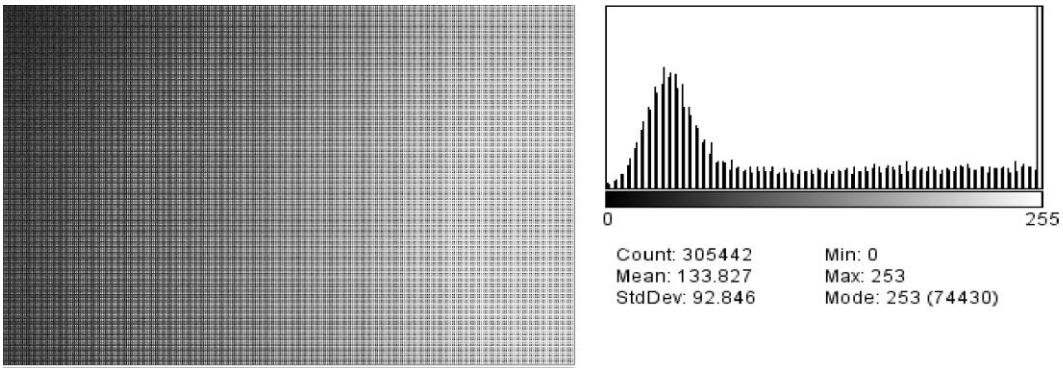


**Figure 39. Actual CCD image for different concetrations of Qdots in alcohol along with histogram of pixel values (no Aperture)**

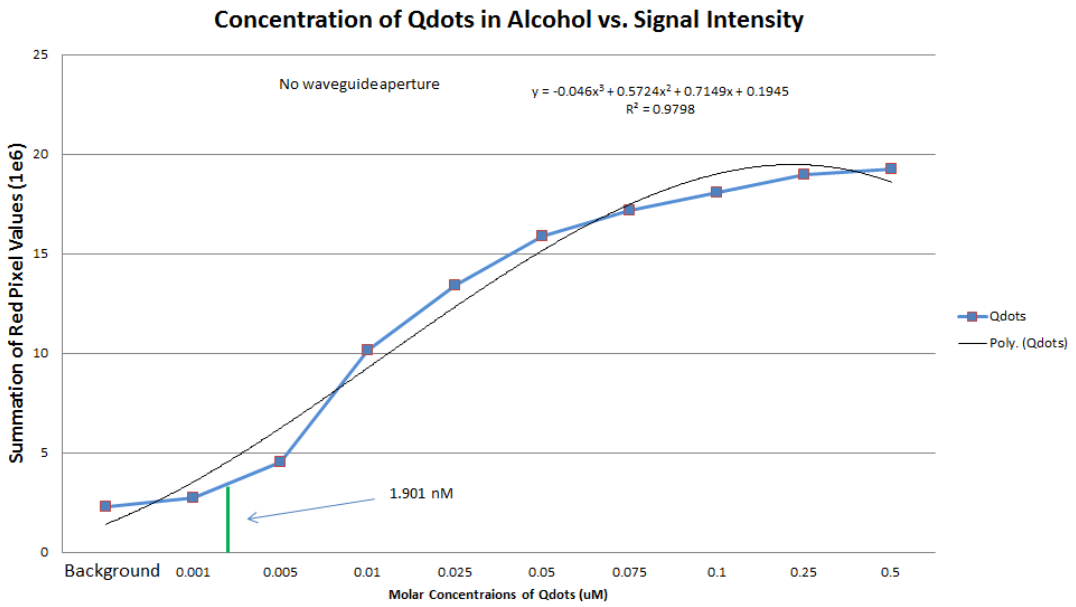


**Figure 40. Concentration of Quantum dots in Alcohol vs. the Signal Intensity No Waveguide Aperture**

As indicated previously, after running some tests the alignment of the waveguide to the excitation light was extremely critical. As a result, a waveguide aperture was designed and placed in front of the waveguide. This aperture made immediate and useful difference in the reliability of the tests, so the same tests were conducted as before but with the waveguide aperture in place. The same molar concentrations of Qdots in Alcohol were used and there was a significant reduction in the LOD. The LOD for this set of tests was 0.0285 nM. This improved LOD indicated that the lens-less CCD is capable of detecting Qdots in a range of some significant biological tests (0.01 nM - 0.1 µM).

Qdot concentration of Background 0 uM

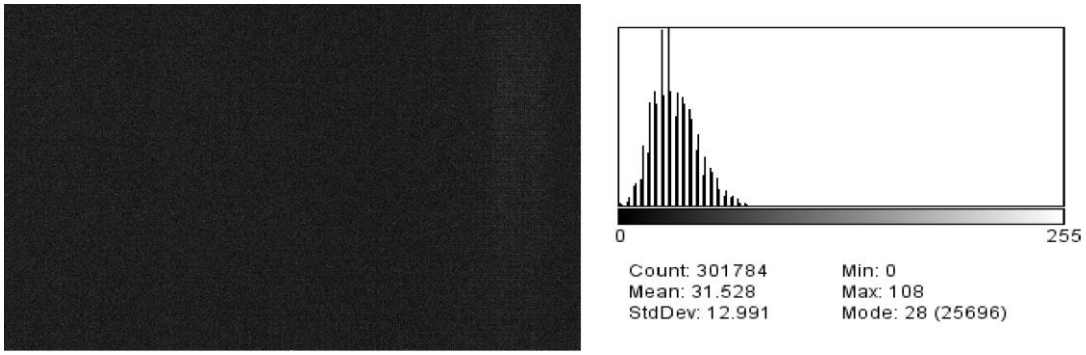


Qdot concentration of 0.001 uM

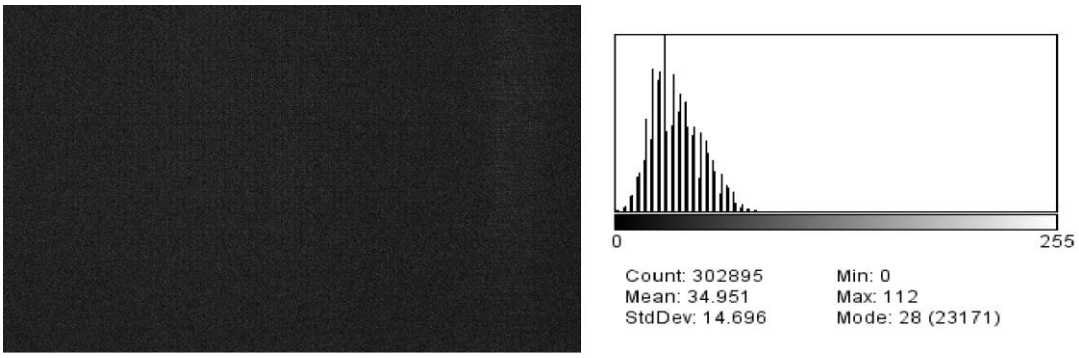


Qdot concentration of 0.005 uM

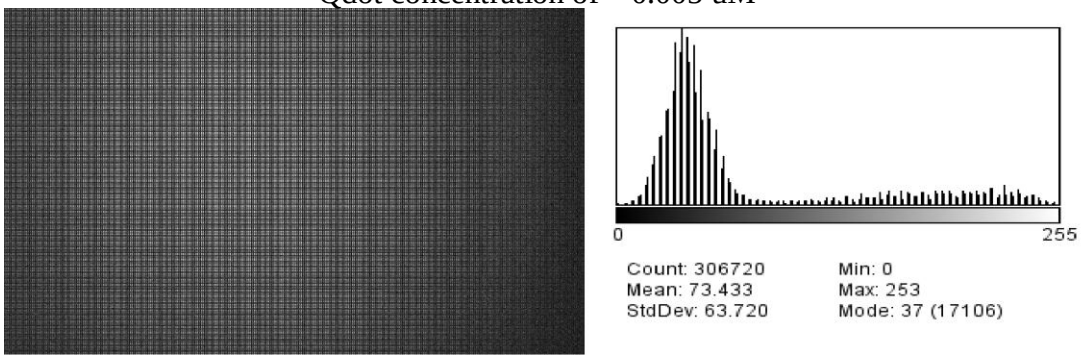


**Figure 41. Actual CCD image for different concetrations of Qdots in alcohol along with histogram of pixel values (with waveguide Aperture)**

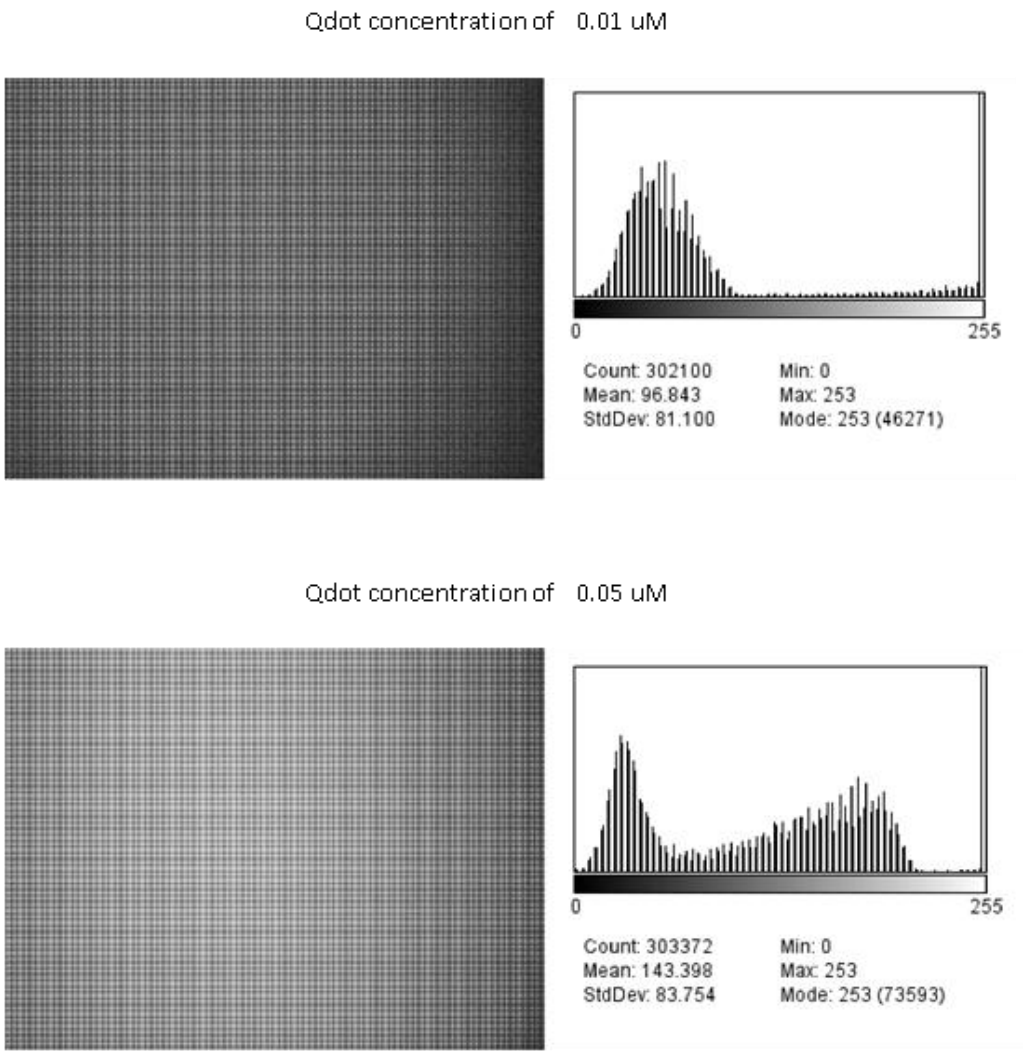


**Figure 42. Actual CCD image for different concetrations of Qdots in alcohol along with histogram of pixel values (with waveguide Aperture)**

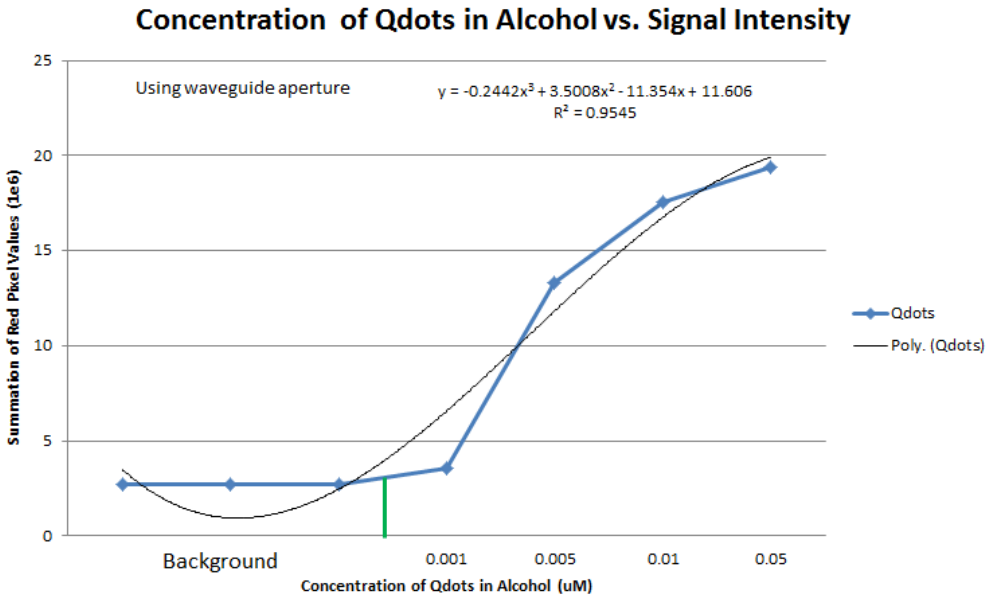


**Figure 43. Concentration of Quantum dots in Alcohol vs. the Signal Intensity using Waveguide Aperture**

A summary of the fluorophores and the different CCD imagers that were used in this research project is shown in Table 1.

**Table 1. Results of LOD for diferent fluorophores and CCD imagers**

| Fluorophore | Light Source (Wavelength) | CCD Imager | Results (LOD) |
|---|---|---|---|
| **Fluorescein** | LED (485 nm) | Logitech C210 Webcam | 52 µM |
| **Fluorescein** | LED (485nm) | Modified Logitech C250 Webcam | Too Much noise created by modifications |
| **Fluorescein** | LED (485 nm) | Fire I remote Head CCD | 36 µM |
| **Phosphor Dots With aperture** | LED (350nm) | Fire I remote Head CCD | 23.10 µM |
| **Coated Qdots in PBS Buffer With aperture** | Laser Diode (405 nm) | Fire I remote Head CCD | 6.38 µM |
| **Functionalized system with Qdots With aperture CRP Test** | Laser Diode (405 nm) | Fire I remote Head CCD | 5.65 µM |
| **Qdots in Alcohol** | Laser Diode (405 nm) | Fire I remote Head CCD | 1.9 nM |
| **Qdots in Alcohol With aperture** | Laser Diode (405 nm) | Fire I remote Head CCD | 0.028 nM |

### 4.2 Fluid Handling and Feedback Control

Handling and feedback control are crucial to the HBLD device working properly. A series of tests was run to determine the optimum lighting conditions for providing accurate and reliable results with the fluorescence optical detection system. The light source was located directly over the lens-less CCD and the detection site. Several different light sources were tested for their ability to provide the best illumination of the detection site.

The first tests evaluated a variety of LEDs with different wavelengths and how accurately the CCD could detect the presence of a clear liquid in the detection zone. Table 2 shows the color of each LED and its corresponding power output as well as its dispersion angle.

**Table 2. Excitation light sources that were tested for feedback control**

| Color Wavelength(ηM) LED | Manufacturer | Part Number | Dispersion Angle (degrees) | Luminous Intensity |
|---|---|---|---|---|
| Red (643) | Jameco | 333973 | 36 | 75mcd |
| Amber Flat (605) | LUMEX | 09J9272 | 110 | 5mcd |
| Amber (596) | CREE | 02P7166 | 30 | 5cd |
| Cool White | VCC | 57P7152 | 100 | 1.8cd |
| Diffuse White | VCC | 50P9329 | 30 | 7cd |
| Cyan (480) | CREE | 04R6672 | 15 | 11cd |
| UV (365) | Cree | 67-2133-ND | 80 | -- |
| Yellow (585) | Vishay | 751-1148-ND | 28 | 10mcd |

The detection of a variety of fluorophores required the use of different optical filters. A series of tests was run to determine the effect of the filters on the ability of

the feedback control system to operate properly while using the different wavelength feedback control light sources. Table 3 shows the various LED light sources and the different filters that were used in the optical detection tests. From Table 3 it can be seen that the only light source that allowed the lens-less CCD to detect a clear liquid was the diffuse white LED.

**Table 3. LED light sources with Optical filters that were tested for the presence of clear liquids**

| | LED Light Source | | | | |
|---|---|---|---|---|---|
| **Optical Filter** | Red | Blue | Amber | White | Diffuse White |
| 607 bandpass Filter | No | No | No | No | Yes |
| 532 10 fwhm | No | No | No | No | Yes |
| Wratten no 12 | Yes | Yes | Yes | No | Yes |
| Square bandpass filter | No | Yes | No | No | Yes |
| 483 bandpass 31 ηM | No | No | No | Yes | Yes |
| 500 ηM Longpass | No | No | No | No | Yes |

| | LED Light Source | | | |
|---|---|---|---|---|
| **Optical Filter** | UV | Green | yellow | flat amber |
| 607 bandpass Filter | Yes | No | No | Yes |
| 532 10 fwhm | No | No | No | No |
| Wratten No 12 | No | No | No | Yes |
| Square bandpass filter | No | No | No | Yes |
| 483 bandpass 31 ηM | No | No | No | No |
| 500 ηM Longpass | No | No | No | Yes |

All the LED light sources were also subjected to a test to determine the effective distances from the top of the microfluidic chip. Table 4 shows the results from the cool white LED minimum distance tests. In this table, a "0" denotes that the edges of the LOC detection site were not able to be detected and the pump was not

turned on. A "1" means the edge detection section of the algorithm was able to find the ROI and the pumping algorithm was initiated. The lens-less CCD was only able to determine the edges after the white diffuse LED was at a height of 20mm from the top of the PDMS chip. At heights of 25mm and 30mm, the picture acquired from the CCD imager became clearer. This test showed that the farther away from the chip that the LED was, the better the image became. The distance is critical for the design of the HBLD device because this LED is located on the cover above the LOC. The cover of the HBLD is 27.5 mm from the top of the LOC above the minimum height required. These results show that in the HBLD, the distance where the LED was positioned was adequate enough to produce an acceptable image for edge detection and the feedback pumping.

**Table 4. Results of Voltages and Heights for the White Diffuse LED**

| | Distance from Top of LOC chip | | | | | |
|---|---|---|---|---|---|---|
| Voltage (V) | 5 mm | 10 mm | 15 mm | 20 mm | 25 mm | 30 mm |
| 2.4 | 0 | 0 | 0 | 1 | 1 | 1 |
| 2.6 | 0 | 0 | 0 | 1 | 1 | 1 |
| 2.8 | 0 | 0 | 0 | 1 | 1 | 1 |

Once the proper LED and its distance from the LOC was determined, an evaluation of the types of liquids that could be detected was performed. For use in a POC LOC device, all the reagents and samples must be detectable and most of these fluids are clear. The effects of the Qdots in solution also needed to be evaluated to

determine if they would fluoresce in the broad white LED spectrum. Figure 44 shows the ability of the feedback control system to recognize the presence of all the relevant bio-reagents tested. The lens-less CCD was able to detect Serum, capture and detection antibodies, PBS PBST, Qdots, FITC, CRP in buffer, and water.

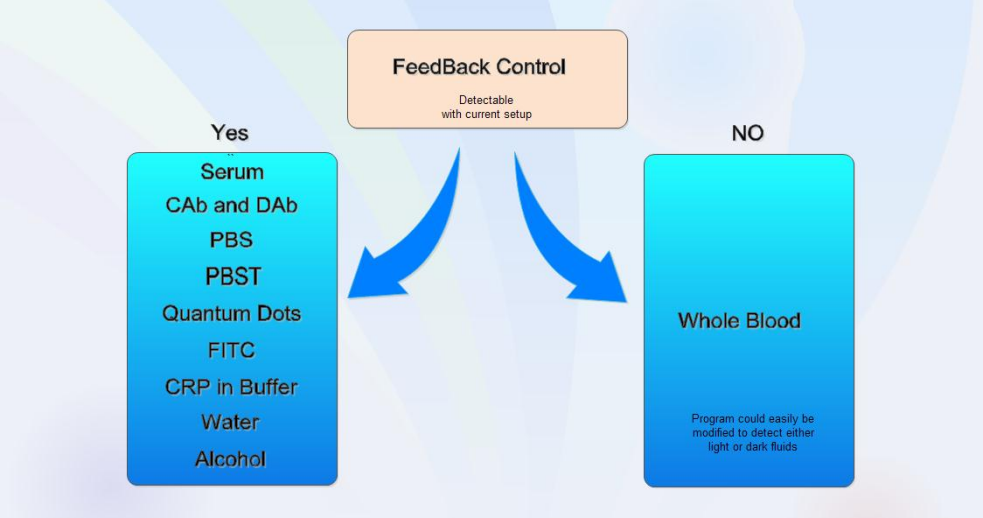


**Figure 44. Fluids that the CCD feedback control system is capable of detecting**

The only fluid that the feedback control system had a difficult time detecting was the whole blood due to the fact that it is not a clear liquid. The feedback control system has the ability to differentiate between dark and light. However the program that was used was only looking for a clear fluid.

All of the above having been considered, at the beginning of an actual test, a control image is taken. This image is compared with a later image to determine whether air or a liquid is in the detection chamber. When the feedback control is started, an image is then to be taken every 0.20 seconds. Each image is subsequently compared to the original control image by contrasting the two images. A threshold

value (normally between 10 to 16) is used and every element in the new subtracted matrix is compared to the threshold value. If this threshold value is too small, then typically the amplitude of the noise will overpower any change in the detection site, and the CCD imager might react to false positives. If the threshold value is too high, then the camera is not sensitive enough and will not change what happens in the detection chamber. Typically, it is acceptable to have a small amount of noise (about 1-2% of the region of interest) for an accurate and sensitive pumping cycle. If the compared pixel values are less than the threshold value, the pixel value is set to 255(white) otherwise it is set to 0(black), these values create a binary mask.

After the binary mask is created, the white and black pixels values are added up. If there are more black pixels than white pixels, it means there was a change and there is now air in the chamber. However, if there are more white pixels than black pixels, it means there is still no change from the initial state, and therefore there is still liquid in the chamber. After air has been found, the program will change from looking to a majority of black pixels to looking for a majority of white pixels. A sample of the time lapse images in the detection chamber illustrating the changes is shown in Figure 45. The figure show the initial state of the detection site and the ROIs filled with a liquid. After t=0.5 s the air plug is beginning to fill the detection site. At time t=2.0 s the entire detection site is filled with air, and the computer algorithm is now checking for a change in state (air to liquid). After t= 9.0s the detection site is completely filled and the test is complete. Note that between time t=2.0s and t= 8.0 the pump was stopped and then restarted.

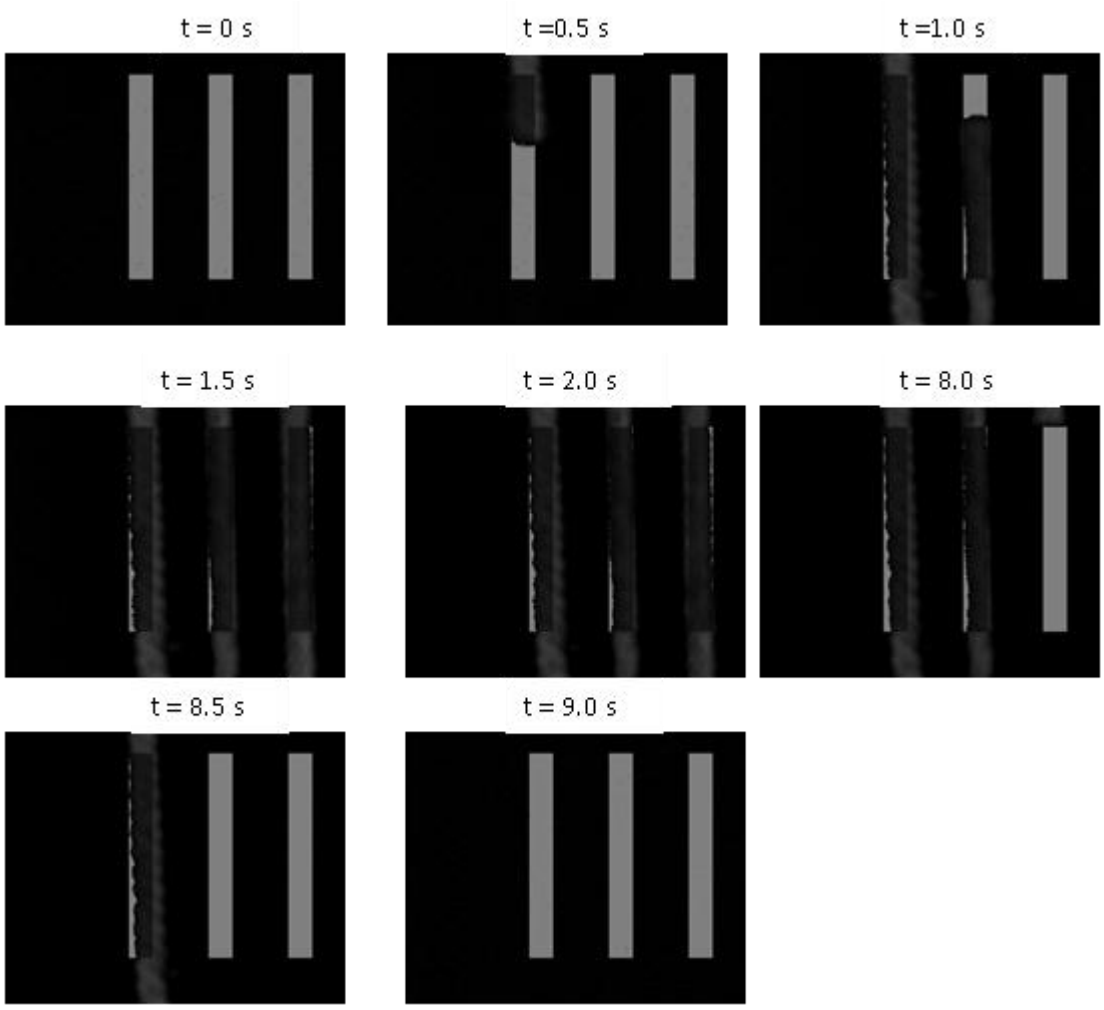


**Figure 45. Time lapse images of fluid moving through S- shaped channel and feedback response**

### 4.3 Smartphone Integration

A unique aspect of the HBLD is its integration with the iPhone. An iPhone App was designed and installed on an iPod Touch. The program that was created can be loaded onto any of the Apple iOS devices (iPhone, iPad, etc.) using X code and interface builder in the iPhone development kit. The iPhone App has the ability to add, store, and delete patient information. This patient directory is stored in a directory called "plist" so that if for any reason the iPhone should go to the main screen, the information that is stored will not be lost. The App has three tabs which are shown in Figure 46 and are identified as: 1) inputting patient/user information, 2) getting test results, 3) using the manual controls and adjusting the settings. The manual control screen, labeled "a" in Figure 46, shows the manual control screen for control of the wireless Arduino microcontroller. The App allows the email settings such as: the passwords, email accounts, and relevant server information to be adjusted. The new iPhone App has the ability to use dynamic host protocol, which is the ability to change the IP address of the server. This ability allows the iPhone and the Arduino to find each other on the server network without knowing the exact IP address. All of these variables are stored in a plist called "NSUserDefaults". This technique provides for ease of storage and sharing data over the multiple lists. In Figure 46 images "b", "c", and "d" show the patient list, the editing of the patient list, and the addition of a new patient. Image "e" shows the appearance of the "Add patient" screen. Image "f" shows the appearance of the screen when a patient from the patient list is selected. On this screen, the user has the ability to choose the test to be run. If no test is selected,

the App will not send the data and it will instead notify the user that in order to start a test a valid choice must be made.

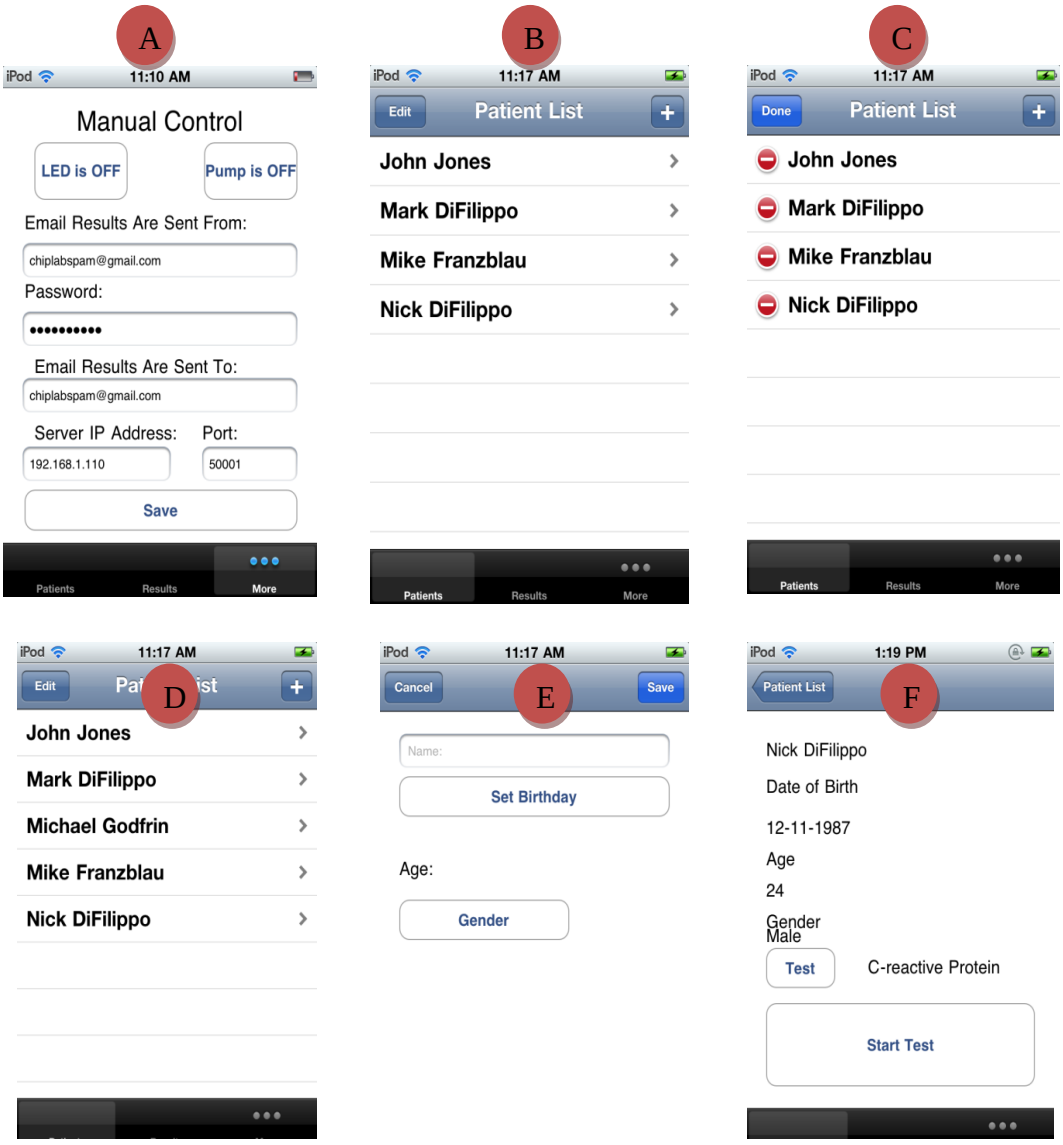


**Figure 46. Custom iPhone App screen shots**

A similar smartphone App was created for a phone running the Android operating system. The following are screen shots from the Android App.

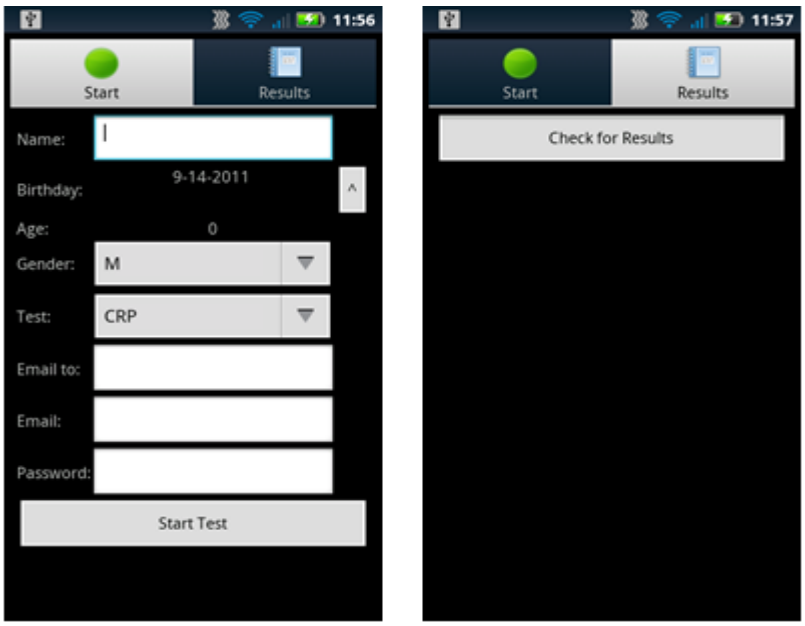


**Figure 47. Custom Android Smartphone App screen shots**

Regardless of the smartphone device, at the completion of the test, the Python program generates a custom report, and emails the results to a predetermined account. Results may also be delivered to the smartphone device for immediate evaluation. Figure 48 shows the custom generated PDF containing the patient's name and the definitive results.

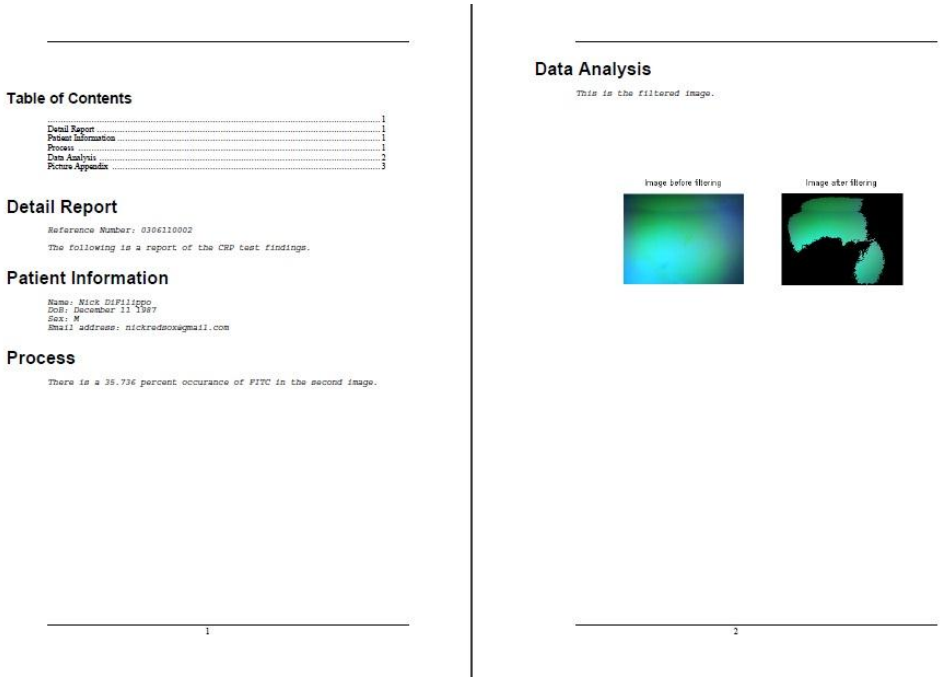


**Figure 48. Custom PDF file generated by Python for results from the HBLD**

## 4.4 Assay protocol

The assay protocol that was used has six steps involving the biological reagents that were discussed in chapter 3. The new LOC chip filled with colored fluid that represents the different preloaded biological reagents can be seen in Figure 49. The green fluid in the detection chamber is a storage buffer that protects the rabbit anti-CRP during storage of the chip. The yellow fluid is the sample fluid to be analyzed and is the only fluid that is not preloaded into the LOC. The blue fluid closest to the detection site is a PBS wash followed by the goat anti-CRP. The final blue fluid is a PBST ( 1x PBS + 0.5 µl/mL Tween 20) wash. The purple fluid is a reference fluid used for accurate qualitative analysis. The air gaps in between the reagents are used for feedback control as well as an aspirate step.

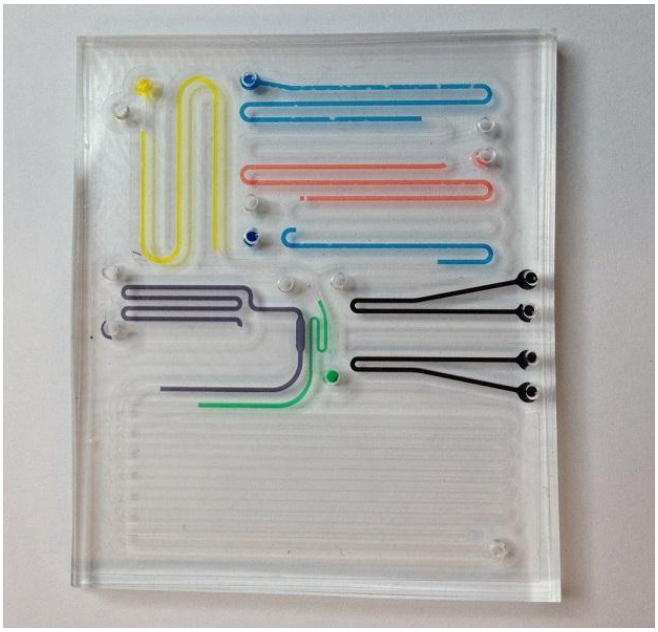

**Figure 49. Custom design chip with fluids indicating various biological reagents**

The limiting factor of microfluidic IFA has been a tradeoff between analysis time and sensitivity. The effect of washing, antigen-antibody reaction, and antigen absorption time on the sensitivity of the assay was investigated [53]. The goal was to decrease the analysis time while maintaining or reducing the LOD [54]. The assay protocol steps that were developed were based on previous kinetics studies by Peng Li. The duration time that each fluid spent in the detection chamber can be seen in Table 5. The yellow section in the table represents the preloaded reagents in the microfluidic chip.

**Table 5. Sequential order of biological reagents and duration of their incubation time**

| Number | Step | Duration |
|---|---|---|
| 1 | Incubate with Rabbit anti-CRP | Preloaded in Chip |
| 2 | Flush with PBS and Aspirate | 10 sec |
| 3 | Incubate Sample | 5 min |
| 4 | Flush with PBS and Aspirate | 10 sec |
| 5 | Incubate with Goat anti-CRP | 5 min |
| 6 | Flush with PBS and Aspirate | 5 min |
| 7 | Incubate Quantum Dots | 5 min |
| 8 | Flush with PBS and Aspirate | 5 min |
| 9 | Wash with PBST | 5 min |
| | Total time of test | 30 min and 20 sec |

In chapter 2,Figure 9, page 21, the brown area represents the analysis time and LOD for an immunofluorescent assay. This region varies between 80 and 500 minutes, and for the biological assay developed for this research the analysis was substantially less than that with an analysis time of 30 minutes and 20 seconds.

There are three additional steps in this biological assay compared to previous IFA assays due to the lack of availability of quantum dot labeled detection antibodies. These additional steps (steps 6, 7 and 8) account for 15 additional minutes that could be eliminated in the future. The entire immunoassay tests are carried out at room

temperature. All the reagents used, as well as the sample, are contained in a disposable LOC. At the completion of each test, the chips can easily be disposed. The pre-functionalized CRP detection chips are stored in a vacuum sealed pouch at between 2° C to 8° C (Figure 50).


**Figure 50. Pre-functionalized ready to run CRP test in vacuum sealed bags**

### 4.5 Hand-held POC Device

Using the HBLD detection device is a straight forward process that can be performed by a consumer or healthcare professional. To operate the HBLD LOC, the sample is loaded onto the sample port of the LOC and is then inserted into the HBLD unit. The LOC has alignment holes that accurately position the LOC in the optimum position above the lens-less CCD.

The alignment pins are actually the interface between the LOC and the POC. The alignment points are the interface between the LOC and the HBLD fluid-

handling-system. Once the chip is securely positioned into the HBLD, the lid can be closed and the device can be powered up by switching the power button on.


**Figure 51. Hand-held lens-less POC LOC device**

Once the unit receives power, a custom HBLD program is activated by either the smartphone App or the touchscreen interface. The HBLD runs a series of diagnostic test prior to starting the actual test. The user then enters the appropriate information such as patient name, date of birth, and the particular test that will be performed into the smartphone App. The tests are completely automated and the user needs only to wait the allotted time for the completion of the test.

Figure 52 shows a comparison of the HBLD to the commonly used Roche CRP detector and the "Shoe box size" APOCIS designed by Dr. Li. The table shows

the compact size and weight of the HBLD as compared to the other two CRP detection devices while maintaining a low LOD. The HBLD is the only detector of the three which has wireless capabilities.

| | Roche | APOCIS | HBLD |
|---|---|---|---|
| **Dimensions** | 72 x 72 x 109 cm<br>0.56 cubic meters | 23 x 15 x 8.5 cm<br>0.00293 cubic meters | 21 x 15 x 6.5 cm<br>0.00133 cubic meters |
| **Weight** | 200 Kg | 1.632 Kg | 0.695 Kg |
| **Automation** | Yes | Yes | Yes |
| **Sample container** | 1.5-10 mL | 5-7 µL | 5-7 µL |
| **Sensitivity** | 0.21 µg/mL | 0.13 µg/mL<br>(in PBS) | 0.13ug/mL<br>(in PBS) |
| **Detection range** | 0.1-20 µg/mL | 0.13-200 µg/mL | 5.65 - 100 µg/mL |
| **Portable** | No | Yes | Yes |
| **Cost per test** | $45 to 85 | $1.50 | $1.50 |
| **Analysis time** | 150 min | 5-20 min | 5-20 min |
| **Wireless** | No | No | Yes |

**Figure 52. Comparison of C-reactive protein detectors**

# CHAPTER 5

## CONCLUSION

It has been demonstrated that the lens-less CCD imager is a viable detector, and the key component of a hand-held detection device. Apart from the Wi-Fi connection, the device is a "stand alone" detector that is compact and portable enough to be used in any setting where Wi-Fi is available.

The genesis of this project began in the 2005-2006 academic year with Dr. Peng Li as the principle researcher. It has now come to fruition in a detection device with several improvements and extensive miniaturization to make the device a viable, marketable product.

Though the total process of this research has been streamlined into only the salient factors, each step has been challenging and required a degree of expertise in computer engineering, electrical engineering, biology, chemical engineering to support the mechanical engineering. The following pages deal with only the major project accomplishments but provide a conclusion as well as some potential adaptations for future (before market) improvements.

### 5.1 Lens-less Detection

The goal of this thesis was to prove that a lens-less CCD imager could be used for the detection of organic and inorganic fluorophores. It was shown that lens-less CCD was able to detect organic and inorganic fluorophores with an LOC. The

comparison of detection devices with a variety of fluorophores and their respective LOD can be seen in Table 6.

**Table 6. Comparison of Photodetectors and Fluorophores with System LOD**

| **Author / Year** | **Light Source** | **Detector** | **Fluorophore** | **LOD** | **POC implementation-Issues** |
|---|---|---|---|---|---|
| Miyaki37 (2005) | LED | PMT | Fluorescein | 120 nM | Low – Optical components are integrated into the Microchip |
| Thrush (2005) | VCSEL | GeAs PD | Phosphoramidite | 40 nM | Good – Optical sensor can be removed from the biochip |
| Mazurcyk (2006) | Nd-YAG laser | SI- PD | Cy3 | 0.5nM | Low – Light source is bulky and expensive |
| Fu (2006) | Laser | PMT | Fluorescein | 1.1 pM | Low - Bulky and expensive off – chip optical elements |
| Liu (2007) | Led | PMT | FITC | 10.1 µM | Low – Optical components are integrated into the microchip |
| Novak ( 2007) | LED | PD | Fluorescein | 1.9 nM | Good – Bio reader is integrated into the bio chip |
| Pais (2008) | OLED | OPD | Fluorescein | 10 µM | Good – Moderate sensitivity, expensive integration costs |
| Mairal (2009) | LED | PD | Rhodamine | 1.4 ng/ml | Good – Simple optical system |
| Li (2010) | LED | Spectrometer | FITC | 22.5 nM | Good - Simple optical system |
| This Work (2012) | Laser Diode | CCD | Quantum Dots | 0.028 nM | Good – Small and inexpensive optical components |

## 5.2 Fluid Handling

The fluid handling system designed for this LOC successfully delivered the biological reagents to the detection site with great reliability. Using the CCD as a detector for the feedback system was essential in achieving this accuracy. Table 7 shows a variety of pumping methods currently being used and the benefits of each method. The pumping system that was employed for this research, which was active with a control system, is very easy to control and extremely accurate. This system does not require difficult procedures to complete a test, because the fluid handling system is completely automated and can be operated by persons without high levels of training.

**Table 7. Comparison of Pumping Methods for Applicaton in a POC Device**

| Researcher (year) | Method | Key Features/Drawbacks |
|---|---|---|
| Gervais (2009) | Capillary Force | Enables one-step, rapid, automated analyses at low cost but this method has limited liquid handling capabilities. In addition, it requires surface modification and sometimes a multi-step fabrication process. |
| Li (2010) | Driven Flow | Allows an automated control of complex fluid delivery but relies on timed movement of fluids (sometimes inaccurate). |
| Kartalov (2006) | Pneumatic | Needs an external gas sources to operate. On-chip micro valves fabricated by multi-layer lithography are needed to segregate different reagents. |

| | | |
|---|---|---|
| Lee (2009) | Centrifugation | Permits a sequential delivery of multiple reagents but needs a rotary motor to provide the centrifugal force. Passive or active on-disc micro valves are needed. |
| Hu (2005)<br>Herr (2007) | Electrophoresis | Has the ability of handling multiple reagents with nL-pL volumes in an automated fashion; however, metal electrodes and an off-chip high voltage sequencer are needed. Also the surface of the microchannels needs to be charged to generate electro-osmosis flow. |
| Pamula (2009) | Electro- wetting | Allows manipulation of individual water droplets but needs integrated micro- electrodes. Oil is often needed as an insulating liquid to encapsulate the reagent-containing water droplets. |
| Li (2010) | μ-VSLS | Allows one-step, rapid, automated analyses at low cost. No on-chip valve or surface charge is needed. This technique has abilities to handle multiple reagents. Relies on timing of reagents to deliver the sequentially loaded LOC. |
| This Work (2012) | Driven Flow | The same ability as system designed by Li, but now has an extremely accurate fluid control due to use of onboard imaging device and fully programmed flow. |

## 5.3 Biological Assay

The biological assay that was performed was accurate at providing reliable results for the detection of CRP. After having run hundreds of biological tests, a pattern emerged showing there was some non-specific binding of the biotinylated Qdots to the functionalized detection site [55]. The theoretical system LOD and the LOD for the detection of CRP were off by a factor of 10 inferring that these non-bound Qdots were responsible for this discrepancy. Assays that were performed with the LOC were limited by the inability to purchase already-labeled detection antibodies. There are no manufactures that could provide the required goat anti-CRP tagged antibodies within the United States. One alternative would be to make one's own labeled detection antibodies to ensure that there are no Qdots in the detection site which are not bound to a respective antibody.

## 5.4 Future Design Enhancements

### 5.4.1 Future Detection Design

As with any design to concept, there are always specific areas that could use improvement. The Fire I lens-less CCD was an accurate and reliable detector for the detection of a variety of fluorophores. An improvement that could dramatically decrease the LOD would be the use of a more sensitive CCD imager designed for scientific purposes. Scientific cameras usually have a large field of view, high spatial resolution, and high dynamic range enabling more pixel information and a better representation of the detection site.

The computer program that was created to analyze the data was successful in detecting a variety of fluorophores; however a new algorithm could be written that would focus in on areas of the detection site that may have clusters of specific fluorophores. The detection of these clusters could fine-tune the accuracy of the results.

When using Qdots, multiplexing is a very popular option because the excitation light is the same for each different fluorophore. Therefore several biological tests could be performed on the same LOC at the same time. The images from lens-less CCD could be used to analyze specific areas of the LOC that contain specific antigen–antibody reactions. This would allow the HBLD to be used as a multifunction detector. The latter is a very important feature due to the fact that most medical providers may well be resistant to purchasing a device that only performs one test.

### S5.4.2 Fluid Handling

The fluid handling system worked extremely well for both the bench-top setup and the HBLD. The main area that needs improvement is the micropump. The Bartels double diaphragm pump used was susceptible to inaccurate pumping due to one or more of the diaphragms sticking. Due to the design of this micropump, it has the capability of pumping liquids better than pumping air. Since all the reagents and samples on the LOC are contained in the waste reservoir, the pump can only pump air making it not as efficient as it could be.

In order to make a disposable LOC without a reader, fluids from the LOC must not contaminate the detection device pumping system. The sample and all the reagents must stay in the LOC. Other types of pumps were tried with no success. A

peristaltic micropump was tried but that pump lacked the power to push or pull the reagents through the length of the LOC at a slow and consistent rate. A syringe pump was very successful at controlling the fluid with consistent flow rates, but that kind of pump is relatively large and difficult to incorporate into a POC device. Some researchers have abandoned the active pumping system that was used in this research and have moved to a passive pumping system such as a pressurized burst pack to push the fluids thru the LOC. Another method of moving the fluids around an LOC is by a "paper based" product "wicking" the liquids through the detection site [56]. This type of system could easily be incorporated into a lens-less hand-held detection device.

### 5.4.3 Communication

The current method of communication for the HBLD to the central server is through the use of Wi-Fi. With the changes that are suggested in section 5.5.5, the information that needs to be sent to the central server would be significantly less. The decrease in transmittable data could easily be sent over a cellular network such as 3G or 4G. This technology would allow the detection device to be used in an area where Wi-Fi and Bluetooth are not easily available.

### 5.4.4 Future Hand-held Design

There is one issue that prevents the HBLD device from being a truly portable device. That limitation is the requirement of the CCD imager to be connected to a computer via a fire wire cable. The information from the CCD is too large to send over a wireless network. There are two possible solutions: the first solution is to change the detector, and the second solution is to have a microprocessor powerful enough to

provide on-board processing. The implementation of a photodiode (PD) could provide similar results with a significant reduction in data. A PD would provide real-time analysis of the detection site, since a CCD requires time to read out all the data from each pixel making results not exactly real-time. A PD is also easier to integrate into a small system due to its significantly smaller size compared to a CCD imager.

The use of a PD is not necessarily the only solution or the best. The case for using the CCD instead of the PD was previously discussed. The current HBLD has an on-board microprocessor that is adequate at performing the current desired tasks; however the use of a more powerful microprocessor such as the Raspberry Pi (which is a tiny computer that runs Linux) can easily be programmed with the Python programming language. The Pi has 256 MB of on-board RAM and a 700MHz ARM chip and is only the size of a credit card. The Pi would allow the HBLD to be completely wireless by performing the same functions that the server program does thus eliminating the constant transfer of images between the server and the POC device. With a more powerful microprocessor all the computation work could be performed on the POC device in its continuing miniaturization.

# BIBLIOGRAPHY

[1] P.C.D. Hobbs. *Building electro-optical systems: making it all work*, volume 71. Wiley, 2011.

[2] D. Litwiller. CCD vs. CMOS. *Photonics Spectra*, 2001.

[3] Adc conversion/, http://learn.hamamatsu.com/tutorials/java/adconversion/date accessed, june 03,2012.

[4] S. Weiss. Fluorescence spectroscopy of single biomolecules. *Science*, 283 (5408): 1676–1683, 1999.

[5] Fluroscence spectroscopy detectors, http://www.tech-faq.com/fluorescence-spectroscopy.html, date accessed june 19,2012.

[6] C.H. Ahn, J.W. Choi, G. Beaucage, J.H. Nevin, J.B. Lee, A. Puntambekar, and J.Y. Lee. Disposable smart lab on a chip for point-of-care clinical diagnostics. *Proceedings of the IEEE*, 92 (1): 154–173, 2004.

[7] B.H. Jo, L.M. Van Lerberghe, K.M. Motsegood, and D.J. Beebe. Three-dimensional micro-channel fabrication in polydimethylsiloxane (pdms) elastomer. *Microelectromechanical Systems, Journal of*, 9 (1): 76–81, 2000.

[8] S.Q. Wang, F. Xu, and U. Demirci. Advances in developing hiv-1 viral load assays for resource-limited settings. *Biotechnology advances*, 28 (6): 770–781, 2010.

[9] T. Laksanasopin, C.D. Chin, H. Moore, J. Wang, Y.K. Cheung, and S.K. Sia. Microfluidic point-of-care diagnostics for resource-poor environments. In *Engineering in Medicine and Biology Society, 2009. EMBC 2009. Annual International Conference of the IEEE*, pages 1057–1059. IEEE, 2009.

[10] Global market for point-of-care diagnostics to reach 16.5 *billion in* 2014, *www.bccresearch.com/pressroom/report/code/hlc*043*c, date accessed june* 2012.

[11] J.Y. Park and L.J. Kricka. Role of nano-and microtechnologies in clinical point-of-care testing. *Handbook of Digital Homecare*, pages 353–362, 2009.

[12] Wifi alliance, www.wi-fi.org, date accessed may 05,2012.

[13] Bluetooth organization,http://www.bluetooth.com/pages/about-technology.aspx, dated accessed may 30,2012.

[14] S.J. Moon, H.O. Keles, A. Ozcan, A. Khademhosseini, E. Hæggstrom, D. Kuritzkes, and U. Demirci. Integrating microfluidics and lensless imaging for point-of-care testing. *Biosensors and Bioelectronics*, 24 (11): 3208–3214, 2009.

[15] A. Ozcan and U. Demirci. Ultra wide-field lens-free monitoring of cells on-chip. *Lab Chip*, 8 (1): 98–106, 2007.

[16] K.K. Ghosh, L.D. Burns, E.D. Cocker, A. Nimmerjahn, Y. Ziv, A. El Gamal, and M.J. Schnitzer. Miniaturized integration of a fluorescence microscope. *nAture methods*, 8 (10): 871–878, 2011.

[17] Y.H. Yang, M.J. Buckley, S. Dudoit, and T.P. Speed. Comparison of methods for image analysis on cdna microarray data. *Journal of computational and graphical statistics*, 11 (1): 108–136, 2002.

[18] G. Durack and J.P. Robinson. *Emerging tools for single-cell analysis: advances in optical measurement technologies*, volume 2. John Wiley and Sons, 2000.

[19] F.B. Myers and L.P. Lee. Innovations in optical microfluidic technologies for point-of-care diagnostics. *Lab Chip*, 8 (12): 2015–2031, 2008.

[20] A.F. Coskun, T.W. Su, and A. Ozcan. Wide field-of-view lens-free fluorescent imaging on a chip. *Lab Chip*, 10 (7): 824–827, 2010.

[21] S.J. Moon, U.A. Gurkan, J. Blander, W.W. Fawzi, S. Aboud, F. Mugusi, D.R. Kuritzkes, and U. Demirci. Enumeration of cd4+ t-cells using a portable microchip count platform in tanzanian hiv-infected patients. *PloS one*, 6 (7): e21409, 2011.

[22] JL Arlett, EB Myers, and ML Roukes. Comparative advantages of mechanical biosensors. *Nature Nanotechnology*, 6 (4): 203–215, 2011.

[23] P. Li, A. Abolmaaty, C. D'Amore, S. Demming, C. Anagnostopoulos, and M. Faghri. Development of an ultrafast quantitative heterogeneous immunoassay on pre-functionalized poly (dimethylsiloxane) microfluidic chips for the next-generation immunosensors. *Microfluidics and nanofluidics*, 7 (4): 593–598, 2009.

[24] U.A. Gurkan, S. Moon, H. Geckil, F. Xu, S. Wang, T.J. Lu, and U. Demirci. Miniaturized lensless imaging systems for cell and microorganism visualization in point-of-care testing. *Biotechnology journal*, 6 (2): 138–149, 2011.

[25] C.P. Price, L.J. Kricka, et al. Improving healthcare accessibility through point-of-care technologies. *Clinical Chemistry*, 53 (9): 1665–1675, 2007.

[26] P. Yager, G.J. Domingo, and J. Gerdes. Point-of-care diagnostics for global health. *Annu. Rev. Biomed. Eng.*, 10: 107–144, 2008.

[27] W.G. Lee, Y.G. Kim, B.G. Chung, U. Demirci, and A. Khademhosseini. Nano/microfluidics for diagnosis of infectious diseases in developing countries. *Advanced drug delivery reviews*, 62 (4-5): 449–457, 2010.

[28] H. Mull. Office of the director, national institute for biomedical imaging and bioengineering national institutes of health july 19, 2010. 2010.

[29] J.L. Platt. Xenotransplantation: recent progress and current perspectives. *Current opinion in immunology*, 8 (5): 721–728, 1996.

[30] P. Yager, T. Edwards, E. Fu, K. Helton, K. Nelson, M.R. Tam, and B.H. Weigl. Microfluidic diagnostic technologies for global public health. *Nature*, 442 (7101): 412–418, 2006.

[31] B. Weigl, G. Domingo, P. LaBarre, and J. Gerlach. Towards non-and minimally instrumented, microfluidics-based diagnostic devices. *Lab Chip*, 8 (12): 1999–2014, 2008.

[32] Abbott point of care, www.abbottpointofcare.com, date accessed may 03 2012.

[33] T.J. Clark, P.H. McPherson, and K.F. Buechler. The triage cardiac panel: Cardiac markers for the triage system. *Point of Care*, 1 (1): 42, 2002.

[34] Biosite triage recall, http://www.yourlawyer.com/topics/overview/biosite-triage-cardiac-panel, date accessed june 03 2012.

[35] BN Feltis, BA Sexton, FL Glenn, MJ Best, M. Wilkins, and TJ Davis. A hand-held surface plasmon resonance biosensor for the detection of ricin and other biological agents. *Biosensors and Bioelectronics*, 23 (7): 1131–1136, 2008.

[36] B.S. Lee, J.N. Lee, J.M. Park, J.G. Lee, S. Kim, Y.K. Cho, and C. Ko. A fully automated immunoassay from whole blood on a disc. *Lab Chip*, 9 (11): 1548–1555, 2009.

[37] J.M. Ruano-López, M. Agirregabiria, G. Olabarria, D. Verdoy, D.D. Bang, M. Bu, A. Wolff, A. Voigt, J.A. Dziuban, R. Walczak, et al. The smartbiophone™, a point of care vision under development through two european projects: Optolabcard and labonfoil. *Lab Chip*, 9 (11): 1495–1499, 2009.

[38] Poc triage cardiac panel, www.alere.com/en_us/ , date accessed june 03,2012.

[39] H.P. Chou, M.A. Unger, and S.R. Quake. A microfabricated rotary pump. *Biomedical Microdevices*, 3 (4): 323–330, 2001.

[40] S.Q. Wang, X. Zhao, I. Khimji, R. Akbas, W. Qiu, D. Edwards, D.W. Cramer, B. Ye, and U. Demirci. Integration of cell phone imaging with microchip elisa to detect ovarian cancer he4 biomarker in urine at the point-of-care. *Lab Chip*, 11 (20): 3411–3418, 2011.

[41] R.A. Boie and I.J. Cox. An analysis of camera noise. *Pattern Analysis and Machine Intelligence, IEEE Transactions on*, 14 (6): 671–674, 1992.

[42] Y. Reibel, M. Jung, M. Bouhifd, B. Cunin, and C. Draman. Ccd or cmos camera noise characterization. *Eur. Phys. J*, 21 (21): 75–80, 2003.

[43] Modifications to ccd for raw data, viewed july 11, 2010.

[44] J. Heikkila and O. Silven. A four-step camera calibration procedure with implicit image correction. In *Computer Vision and Pattern Recognition, 1997. Proceedings., 1997 IEEE Computer Society Conference on*, pages 1106–1112. IEEE, 1997.

[45] Z. Zhang. A flexible new technique for camera calibration. *Pattern Analysis and Machine Intelligence, IEEE Transactions on*, 22 (11): 1330–1334, 2000.

[46] D.A. Armbruster, M.D. Tillman, and L.M. Hubbs. Limit of detection (lqd)/limit of quantitation (loq): comparison of the empirical and the statistical methods exemplified with gc-ms assays of abused drugs. *Clinical chemistry*, 40 (7): 1233–1238, 1994.

[47] A. Piruska, I. Nikcevic, S.H. Lee, C. Ahn, W.R. Heineman, P.A. Limbach, and C.J. Seliskar. The autofluorescence of plastic materials and chips measured under laser irradiation. *Lab chip*, 5 (12): 1348–1354, 2005.

[48] O. Hofmann, X. Wang, A. Cornwell, S. Beecher, A. Raja, D.D.C. Bradley, et al. Monolithically integrated dye-doped pdms long-pass filters for disposable on-chip fluorescence detection. *Lab Chip*, 6 (8): 981–987, 2006.

[49] H. Wu, T.W. Odom, D.T. Chiu, and G.M. Whitesides. Fabrication of complex three-dimensional microchannel systems in pdms. *Journal of the American Chemical Society*, 125 (2): 554–559, 2003.

[50] D.A. Chang-Yen, R.K. Eich, and B.K. Gale. A monolithic pdms waveguide system fabricated using soft-lithography techniques. *Journal of lightwave technology*, 23 (6): 2088, 2005.

[51] P. Garstecki, M.J. Fuerstman, H.A. Stone, and G.M. Whitesides. Formation of droplets and bubbles in a microfluidic t-junction—scaling and mechanism of break-up. *Lab Chip*, 6 (3): 437–446, 2006.

[52] M. Fleger and A. Neyer. Pdms microfluidic chip with integrated waveguides for optical detection. *Microelectronic engineering*, 83 (4): 1291–1293, 2006.

[53] J.G. Erhardt, J.E. Estes, C.M. Pfeiffer, H.K. Biesalski, and N.E. Craft. Combined measurement of ferritin, soluble transferrin receptor, retinol binding protein, and c-reactive protein by an inexpensive, sensitive, and simple sandwich enzyme-linked immunosorbent assay technique. *The Journal of nutrition*, 134 (11): 3127–3132, 2004.

[54] N. Christodoulides, S. Mohanty, C.S. Miller, M.C. Langub, P.N. Floriano, P. Dharshan, M.F. Ali, B. Bernard, D. Romanovicz, E. Anslyn, et al. Application of microchip assay system for the measurement of c-reactive protein in human saliva. *Lab Chip*, 5 (3): 261–269, 2005.

[55] M. Howarth, K. Takao, Y. Hayashi, and A.Y. Ting. Targeting quantum dots to surface proteins in living cells with biotin ligase. *Proceedings of the National Academy of Sciences of the United States of America*, 102 (21): 7583, 2005.

[56] H Chen. Supporting information for a fluidic diode, valves and a sequential-loading circuit fabricated on layered paper. *The Royal Socitey of Chemistry*, Lab on chip, 2012.